CHALMERS
UNIVERSITY OF TECHNOLOGY

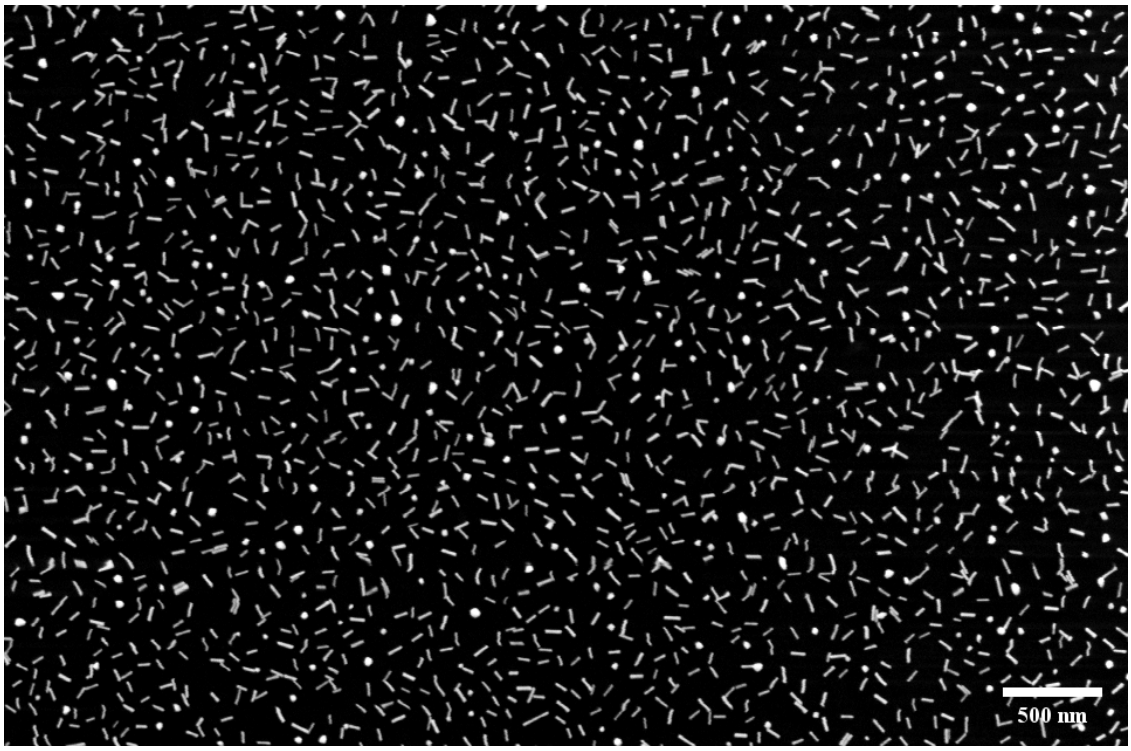

Gold Nanorod-Functionalised Surfaces for Bacterial Elimination

Utilising Localised Surface Plasmon Resonance Generated Heat to Prevent Implant-Associated Infections

Master's thesis in Materials Chemistry

CAROLINE RIDDERSTRÅLE

Department of Chemistry and Chemical Engineering

CHALMERS UNIVERSITY OF TECHNOLOGY
Gothenburg, Sweden 2022
www.chalmers.se

Master's thesis 2022

Gold Nanorod-Functionalised Surfaces for Bacterial Elimination

Utilising Localised Surface Plasmon Resonance Generated Heat to Prevent Implant-Associated Infections

Caroline Ridderstråle

CHALMERS
UNIVERSITY OF TECHNOLOGY

Department of Chemistry and Chemical Engineering
Division of Applied Chemistry
M. A. Research Group
Chalmers University of Technology
Gothenburg, Sweden 2022

Gold Nanorod-Functionalised Surfaces for Bacterial Elimination
Utilising Localised Surface Plasmon Resonance Generated Heat to Prevent Implant-Associated Infections
Caroline Ridderstråle

Supervisor: Maja Uusitalo, Department of Chemistry and Chemical Engineering
Examiner: Martin Andersson, Department of Chemistry and Chemical Engineering

Master's Thesis 2022
Department of Chemistry and Chemical Engineering
Division of Applied Chemistry
M. A. Research Group
Chalmers University of Technology
SE-412 96 Gothenburg
Telephone +46 31 772 1000

Cover: Scanning electron microscopy micrograph at 50 000x magnification of a gold nanorod-functionalised glass surface

Typeset in LaTeX
Printed by Chalmers Reproservice
Gothenburg, Sweden 2022

Gold Nanorod-Functionalised Surfaces for Bacterial Elimination
Utilising Localised Surface Plasmon Resonance Generated Heat to Prevent Implant-Associated Infections
CAROLINE RIDDERSTRÅLE
Department of Chemistry and Chemical Engineering
Chalmers University of Technology

Abstract

Medical implant-associated infections are a major problem in today's healthcare. A big issue is microbial contamination of the implant during surgery, since it often is the start of implant-associated infections. Control of the hospitalisation environment and use of antibiotics have been a key target to minimise the risk of infection during implant surgeries. However, a possible alternative way to inhibit microbial adhesion and growth of bacteria on the implant is to modify the chemistry or the topology of the implant surface. Therefore, to be able to prevent implant-associated infections, the development of new materials is important. A procedure for making use of gold nanorod-functionalised surfaces that are irradiated with near-infrared (NIR) light to photothermally eliminate bacteria in contact with the surfaces has been developed and evaluated in this thesis. The gold nanorod-functionalised surfaces were produced by electrostatic surface assembly of gold nanorods on glass surfaces, and the used gold nanorods were synthesised through a seed-mediated synthesis.

Two types of *in vitro* studies were conducted to evaluate the antimicrobial activity of the gold nanorod-functionalised glass surfaces irradiated with NIR light at 808 nm. From both of the *in vitro* studies the results indicated that a surface with gold nanorods irradiated with NIR light can photothermally eliminate bacteria in contact with the surface. One study contained exposure of the surfaces in a laboratory room to collect microbial contamination on the surfaces, to mimic the exposure of an implant during a surgical procedure. This study also showed that a surface with gold nanorods attracts more particles with bacteria compared to a glass surface, likely due to the electrostatic charge of the gold nanorods. The other *in vitro* study used *Staphylococcus aureus* cultured and partly dried on the surfaces. Approximately 22 % more dead bacteria were detected on the surfaces irradiated with NIR light compared to the control surfaces.

The concept of utilising gold nanorod-functionalised surfaces in combination with NIR light to help fight and prevent implant-associated infections showed promise for future work. It would further be interesting to find an optimum of antimicrobial activity by varying the gold nanorod surface coverage and the power of the NIR laser. Furthermore it would be interesting to expose surfaces in operating rooms for implants, to evaluate the elimination of the microbial contamination occurring in a clinical environment.

Keywords: Gold nanorods, implant-associated infections, localised surface plasmon resonance, antimicrobial surfaces.

Acknowledgements

First and foremost, I would like to thank my examiner Martin Andersson for his advice and support, and also for giving me the opportunity to work with this master's thesis. I am also really grateful to my supervisor Maja Uusitalo for her valuable support, feedback and assistance. Thank you, without all your help with the microbiology studies I couldn't have succeeded in completing this project. I would also like to thank Mats Hulander and Frans Stålfelt for helping me and giving me insight. In addition to that, I would like to thank the rest of the members of M. A. Research Group for welcoming me into the team. Last but not least, I would like to thank my family, friends and everyone who helped and motivated me to work on this master's thesis.

Caroline Ridderstråle, Gothenburg, June 2022

Contents

List of Figures **xi**

List of Tables **xiii**

1 Introduction **1**
1.1 Aim . . . 2
1.2 Limitations . . . 2

2 Theory **3**
2.1 Implant-Associated Infections and Antimicrobial Resistance . . . 3
2.1.1 Airborne Pathogens That Cause Implant-Associated Infections 4
2.1.2 Colony-Forming Unit . . . 4
2.2 Gold Nanorods . . . 5
2.2.1 Seed-Mediated Synthesis of Gold Nanorods . . . 5
2.2.2 Electrostatic Self Assembly of Gold Nanorods on Glass Substrates . . . 7
2.2.3 Localised Surface Plasmon Resonance Frequency of Gold Nanorods 7
2.2.4 Toxicity of Gold Nanorods . . . 9

3 Methodology **11**
3.1 Materials . . . 11
3.2 Synthesis and Purification of Gold Nanorods . . . 11
3.2.1 Synthesis of Gold Nanorods . . . 12
3.2.2 Purification of Gold Nanorods . . . 12
3.3 Surface Assembly of Gold Nanorods . . . 12
3.4 Photothermal Heating of Gold Nanorods Immobilised on Glass . . . 13
3.5 *In Vitro* Studies of Photothermal Elimination . . . 13
3.5.1 Microbial Contamination From Surface Exposure in Laboratory Room . . . 13
3.5.2 Bacteria Cultured on Gold Nanorod-Functionalised Glass . . . 14
3.6 Analytical Techniques and Characterisation . . . 15
3.6.1 UV-Vis-NIR Spectroscopy . . . 15
3.6.2 Scanning Electron Microscopy . . . 16
3.6.3 Fluorescence Microscopy . . . 17

4 Results and Discussion **19**
4.1 Characterisation of Gold Nanorods 19
4.1.1 Localised Surface Plasmon Resonance Spectra of Gold Nanorods in Aqueous Dispersion and Immobilised on Glass 19
4.1.2 Dimensions of Gold Nanorods 20
4.1.3 Surface Coverage of Gold Nanorods Immobilised on Glass . . . 20
4.1.4 Photothermal Heating of Gold Nanorods Immobilised on Glass 22
4.2 *In Vitro* Studies of Photothermal Elimination 22
4.2.1 Microbial Contamination From Surface Exposure in Laboratory Room 22
4.2.1.1 Results Using Near-Infrared Light Irradiation at 10 W 23
4.2.1.2 Results Using Near-Infrared Light Irradiation at 15 W 24
4.2.2 Bacteria Cultured on Gold Nanorod-Functionalised Glass . . . 25

5 Conclusion **29**

Bibliography **31**

A Appendix **i**
AI Calculation of the Gold Nanorod Concentration From UV-Vis-NIR Spectroscopy i
AII Theoretical Calculation of the Gold Nanorod Concentration ii
AIII Gold Nanorod-Functionalised Glass With a Localised Surface Plasmon Resonance Frequency at 742 nm in Air iii

B Appendix **iii**
BI Colony-Forming Unit From the Microbial Contamination Trials . . . iii
BII P-Values of the T-Tests for the Microbial Contamination Trials . . . iv
BIII Statistical Calculations for the Microbial Contamination Trials v
BIV Analysis of Variance Tables for the Microbial Contamination Trials . viii
BV P-Values of the T-Tests for the *In Vitro* Study With Bacteria Cultured on Gold Nanorod-Functionalised Glass ix

List of Figures

2.1 Chemical structure of hexadecyltrimethylammonium bromide (CTAB) 6
2.2 Illustration of electrostatic assembly of gold nanorods on a negatively charged glass surface 7
2.3 Transverse and longitudinal absorption bands illustrated in localised surface plasmon resonance spectrum of gold nanorods 8

4.1 Localised surface plasmon resonance spectra of gold nanorod-functionalised glass measured in air (AuNR-Glass) and gold nanorods dispersed in Milli-Q water (AuNR) 20
4.2 Scanning electron microscopy micrographs of gold nanorod-functionalised glass at 50 000x magnification, shown for both large (a) and small (b) substrates 21
4.3 Images from fluorescence microscopy with a 40x magnification of samples stained with LIVE/DEAD™ from the *in vitro* study with *Staphylococcus aureus* cultured on gold nanorod-functionalised glass 26
4.4 Percentage and standard deviation of dead bacteria covering the surfaces from the *in vitro* study with *Staphylococcus aureus* cultured on gold nanorod-functionalised glass 27

A1 Scanning electron microscopy micrograph at 50 000x magnification of gold nanorod- functionalised glass with a localised surface plasmon resonance frequency of 742 nm measured in air i
A2 Localised surface plasmon resonance spectra of gold nanorod-functionalised glass measured in air (AuNR-Glass^{742}) and gold nanorods measured in Milli-Q water (AuNR^{742}) i

B1 Example pictures of agar plates with colonies after 24 h and 48 h from the trial with near-infrared light at 15 W iii

List of Tables

4.1 Length, width and aspect ratio of gold nanorods with standard deviation 20

4.2 Average surface coverage with standard deviation for both large and small surfaces 21

4.3 Average temperature increase with standard deviation for gold nanorod-functionalised glass (AuNR-Glass) and bare glass (Glass) after irradiation with near-infrared light at 10 W and 15 W 22

4.4 The average number of colony-forming unit with standard deviation for bare glass surfaces (Glass) and gold nanorod-functionalised glass surfaces (AuNR-Glass), either non-irradiated or irradiated with 10 W at 808 nm (+ NIR) 23

4.5 The average number of colony-forming unit with standard deviation for bare glass surfaces (Glass) and gold nanorod-functionalised glass surfaces (AuNR-Glass), either non-irradiated or irradiated with 15 W at 808 nm (+ NIR) 24

B1 Colony-forming unit (CFU) after 24 h and 48 h, where CFU after 48 h is shown in parenthesis, for bare glass surfaces (Glass) and gold nanorod-functionalised glass surfaces (AuNR-Glass), either non-irradiated or irradiated with 10 W at 808 nm (+ NIR) iv

B2 Colony-forming unit (CFU) after 24 h and 48 h, where CFU after 48 h is shown in parenthesis, for bare glass surfaces (Glass) and gold nanorod-functionalised glass surfaces (AuNR-Glass), either non-irradiated or irradiated with 15 W at 808 nm (+ NIR) iv

B3 P-values of each t-test for the microbial contamination trial using near-infrared light at 10 W v

B4 P-values of each t-test for the microbial contamination trial using near-infrared light at 15 W v

B5 The data obtained for the microbial contamination trial with near-infrared light irradiation at 10 W and colony-forming unit counted after 48 h vi

B6 The factor effects for both microbial contamination trials (near-infrared light irradiation at 10 W or 15 W) with colony-forming unit counted after 24 h and 48 h vii

B7 ANOVA table for the microbial contamination trial with near-infrared light irradiation at 10 W with colony-forming unit counted after 24 hours . . . viii
B8 ANOVA table for the microbial contamination trial with near-infrared light irradiation at 10 W with colony-forming unit counted after 48 hours . . . viii
B9 ANOVA table for the microbial contamination trial with near-infrared light irradiation at 15 W with colony-forming unit counted after 24 hours . . . viii
B10 ANOVA table for the microbial contamination trial with near-infrared light irradiation at 15 W with colony-forming unit counted after 48 hours . . . ix
B11 P-values of each t-test for the *in vitro* study with bacteria cultured on gold nanorod-functionalised glass . . . ix

1

Introduction

There is a need for development of ways to replace antibiotics due to increasing occurrence of antimicrobial resistance in the world. Medical implant-associated infections are a major problem since there often is need for long antibiotic treatments and operations for exchange of the implant [1]. Tackling antimicrobial resistance is an ethical obligation. Without preventive action and development of replacements, infections that have been treatable over the past century will condemn to infections with high risk of fatal outcome. Development of new approaches to be able to prevent implant-associated infections are therefore important.

Microbial contamination on an implant from the surgical procedure is often the start of implant-associated infections [2]. Biofilm formation starts with bacterial adhesion to the surface, followed by microcolony formation and biofilm maturation with detachment of bacterial cell [3]. Bacteria in biofilm have higher resistance to the immune system of the infected host and to antibiotics [1]. This higher resistance is the reason why implant-associated infections are very hard to treat.

Gold nanorods of certain aspect ratios exhibit localised surface plasmon resonance (LSPR) upon irradiation with near-infrared (NIR) light, which generates heat that can kill bacteria [4]. The gold nanorods can be synthesised to have their plasmon resonance frequency in the NIR light region, making the nanorods suitable for clinical applications since aqueous tissue absorbs relatively little light in the NIR window between 700 and 1200 nm [5].

A material with gold nanorods on the surface may in the future be a good material to use for medical implants. A glass surface with gold nanorods has previously been shown to photothermally eliminate bacteria growing on the surface [4]. It is further interesting to see how the surrounding environment and the microorganisms in the air that deposits on the surface affect the surface and its efficiency to kill bacteria. Thereby it is of interest to mimic the exposure an implant would have during a surgical procedure. This is also of high clinical relevance for the aimed future application of gold nanorods as a surface material on implants.

1.1 Aim

The aim of this thesis is to investigate the antimicrobial activity of gold nanorod-functionalised glass surfaces with prior contamination from exposure and after culturing of bacteria on the surfaces. This thesis work will provide knowledge on how well the surfaces can eliminate microbial contamination, which will be useful for material development and for future implementation of the material. From a societal aspect, this project could help the development of products that make an impact to create better life quality for humans and fight antimicrobial resistance.

1.2 Limitations

There are several ways to produce gold nanorods. However, only one method will be used in this project. The gold nanorods will be produced through wet-chemical and seed-mediated growth synthesis. The synthesis utilises hexadecyltrimethylammonium bromide (CTAB) as a capping agent on the nanoparticles. Other types of capping agents used for stabilising nanoparticles will not be applied. Only rod-shaped gold nanoparticles will be evaluated in the project. The nanorod-functionalised surfaces that will be evaluated in the project will only include glass substrates. Glass substrates functionalised with gold nanorods have previously been used to show photothermal elimination of bacteria upon irradiation with near-infrared light [4] and is therefore used.

The evaluation on how well gold nanorod-functionalised surfaces can eliminate microbial contamination will only be estimated with two *in vitro* studies. One study will be performed to evaluate how well gold nanorod-functionalised surfaces can eliminate microbiological contamination from prior exposure in laboratory rooms. The other study will evaluate how well gold nanorod-functionalised surfaces can eliminate bacteria cultured on the surfaces. No implantation and *in vivo* studies will be carried out. *Staphylococcus aureus* (*S. aureus*) will be the only bacterial species used for culturing on the surfaces in the microbiological studies. *S. aureus* is used since it is one of the most frequently detected pathogens connected to implant-associated infections [3]. The main evaluation methods to evaluate the antimicrobial activity will be colony-forming unit (CFU) and live-dead staining with fluorescence microscopy. Species identification of the airborne bacteria from the exposure to laboratory room environment will not be done since it is beyond the scope and aim of this project.

2

Theory

This chapter includes theoretical background on implant-associated infections, antimicrobial resistance, airborne pathogens, colony-forming unit, and gold nanorods.

2.1 Implant-Associated Infections and Antimicrobial Resistance

Medical devices such as implants have been used broadly in most fields of medicine. The risk with usage of them are worth considering, particularly when they are implanted inside the body [6]. A big issue is microbial contamination of the implant, surgical wounds during surgery or during the time of hospitalisation. Microbial contamination on the implant from the surgical procedure is often the start of implant-associated infections [2]. The microbial contamination impacts both the patient health and costs related to fight the infection. Microorganisms take advantage of the weakened immune response at the implant surface–tissue interface [1]. When a foreign material is inserted at the surgical site, the critical amount of microorganisms needed to induce an infection is much lower. Microorganisms, such as bacteria, that can form a biofilm on the surface have higher resistance to the body's defense and against antibiotic treatments [1]. Compared to planktonic bacteria may bacteria in a biofilm be 500–5000 times more tolerant to antimicrobial treatments [3]. Mechanisms such as poor antibiotic penetration due to biofilm matrix barrier contribute to biofilm resistance to antimicrobials. The biofilm is also more resistant to the immune system due to that bacterial protecting exopolysaccharides are produced and shelter the bacteria [6]. Biofilm formation starts with bacterial adhesion to the surface, followed by microcolony formation and biofilm maturation with detachment of bacterial cell [3].

Infected implants usually require surgical removal combined with long-term antibiotic treatment [3]. Solely prolonged treatment with high doses of antibiotics are usually not enough to put an end to implant infections. Antibiotics have been the main alternative to fight infections in general. However, antibiotic resistant strains, for example Methicillin-resistant *Staphylococcus aureus* (MRSA) that often are responsible for infections originating in hospitals, are of great concern [6]. Methods used to reduce the microbial contamination include surgical gowns, laminar air flow,

ultraviolet light and limiting room traffic. Solutions with technical ventilation like laminar air flow, are important. However, ventilation systems do not guarantee clean air due to factors like organisation of the work and staff behavior [7]. Control of the environment, contamination from personnel and use of antibiotics have been key strategies to minimise the risk of infection during implant surgeries. A promising alternative way to inhibit microbial adhesion and growth is to modify the chemistry or the topology of the implant surface [1].

2.1.1 Airborne Pathogens That Cause Implant-Associated Infections

Microorganisms causing implant-associated infections are transported on particles in the air and enter surgical sites. The primary source of airborne microorganisms are from people, door openings and room traffic in the operating room [8]. People are emitting dead skin, body vapours, skin oils and microorganisms. The average person sheds 1000 million skin cells per day and approximately 10 % of the skin cells carries microorganisms [9]. The size of airborne particles has impact on their tendency to settle on surfaces. Particles with a size smaller than 5 µm tend to be suspended in the air, while particles larger than 100 µm settle quickly [10]. Depending on the source of the particle, it may carry a variable amount of bacteria. Bacteria have a typical length of 0.2 to 5 µm [10]. They adhere to particles, often those of larger size, and form aggregates.

Pathogens that are causing infections on implants most frequently are detected as *Staphylococcus aureus* (*S. aureus*) and *Staphylococcus epidermidis* (*S. epidermidis*) [3]. Both *S. aureus* and *S. epidermidis* are Gram-positive bacteria [11] and they exhibit several mechanisms of attachment and biofilm formation [2]. Both pathogens can be found on human skin. *S. epidermidis* is a common flora on human skin [12] and about 30% of the human population is colonised with *S. aureus* [13]. Between the two pathogens are implant-associated infections caused by *S. aureus* more severe. *S. epidermidis*, on the other hand, has better access as an opportunistic pathogen since it occurs much more frequently on human skin [11].

2.1.2 Colony-Forming Unit

Colony-forming unit (CFU) is a measurement of how many viable bacteria there are in a sample. It is achieved by counting the amount of colonies that have grown on an agar plate. CFU is often used to determine concentrations of bacteria. This is done by diluting a sample and spreading 50-100 mL of each dilution onto agar plates [14]. Following incubation colonies are counted and bacterial concentration in the original sample can be estimated. When counting it is not certain if the colony arises from one cell or a cell group and results expressed in CFU reflect this uncertainty.

2.2 Gold Nanorods

Unique geometry dependent electronic, chemical and tunable optical properties distinguish nanoscale gold to other nanoparticles [15]. Gold nanorods have gotten attention in research due to their tunable plasmonic properties and compatibility for diverse applications. Some application areas of gold nanorods are solar harvesting, sensing, surface-enhanced spectroscopy, and photothermal therapy [16]. The interesting properties of gold nanorods arise from the phenomena of localised surface plasmon resonance (LSPR). Control over the nanorods aspect ratio (length/width) allows for tuning of the plasmon resonances over a visible to near-infrared (NIR) spectral span [17].

2.2.1 Seed-Mediated Synthesis of Gold Nanorods

Seed-mediated growth of monodisperse colloidal particles is one of the most common methods for synthesis of nanoparticles. This type of synthesis method dates back to the 1920s [18]. There are several approaches to produce gold nanorods other than seed-mediated growth methods, both bottom up and top down procedures. For example, some other bottom up approaches are electrochemical synthesis and ultraviolet photochemical reduction of gold salts [5]. Top down approaches used for production of gold nanorods are lithographic fabrication and template assessed synthesis.

Seed-mediated synthesis of gold nanorods is a popular method due to its relative simplicity and use of inexpensive materials [18]. It gives high quality and a high yield of nanorods. The seed-mediated synthesis is also preferred since it is easy to influence the shape and size of the nanorods by changing parameters, such as concentration, in the synthesis protocol. The first step of the synthesis is creating a seed solution where nucleation of small gold nanospheres happens. This seed solution often consists of gold(III) chloride trihydrate ($HAuCl_4 \cdot 3H_2O$), sodium borhydride ($NaBH_4$), and hexadecyltrimethylammonium bromide ($CH_3(CH_2)_{15}N(Br)(CH_3)_3$) also referred to as CTAB. The small gold nanospheres produced in the seed solution are then added to a growth solution were the nanoparticles grow into rod-shapes. The growth solution usually consists of CTAB, $HAuCl_4$, hydrochloric acid (HCl), silver nitrate ($AgNO_3$), and L-ascorbic acid.

The gold goes through three different oxidation states during the seed-mediated synthesis. The precursor is Au(III) from $HAuCl_4$. $NaBH_4$ is used as a strong reducing agent for the production of the gold seeds, reducing Au(III) to Au(0). L-ascorbic acid is a weak reducing agent and is used in the growth solution to reduce Au(III) to Au(I). A weak reduction agent is needed to ensure that the final reduction step only takes place on the existing nuclei in the solution. L-ascorbic acid can reduce gold to Au(0) if metal nanoparticles that catalyse the reaction are present [19]. Therefore, in the addition of the seed solution to the growth solution the seeds are catalysing the final reduction, inducing deposition of Au(I) on the seed surface only [16]. The concentration of the weak reducing agent L-ascorbic acid influences the aspect ratio

(length/width) of the gold nanorods. A lower concentration will increase the aspect ratio [16].

The capping agent used to stabilise the particles in the synthesis is often CTAB. CTAB is known to form rod-shaped micelles at certain concentrations and have a carbon tail that is long enough to stabilise the nanorods but still short enough to have solubility close to room temperature [16]. The chemical structure of CTAB is presented in Figure 2.1. The particles are stabilised from aggregating when they are capped with CTAB and they have a net positive surface charge due to the cationic ammonium head group of CTAB. The seed-mediated synthesis of gold nanorods requires both thermodynamic and kinetic control. A ligand exchange occurs for $HAuCl_4$ when CTAB is used. The bromide counterions of the surfactant CTAB will replace the chloride in $HAuCl_4$ due to the complexation strength of Au(III). The change of ligands and ion pair formation of $HAuBr_4^-$ with the quaternary ammonium surfactant monomers (CTA^+) will create a variation in the redox potentials that influence the growth kinetics [16]. It is therefore important that the ligand exchange is completed before the gold nanorod growth starts.

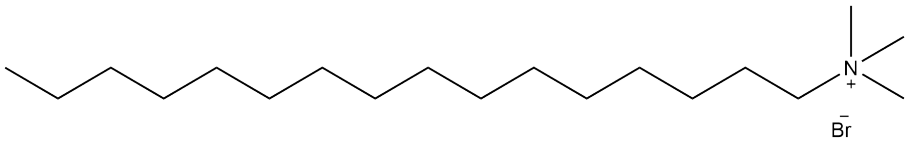

Figure 2.1: Chemical structure of hexadecyltrimethylammonium bromide (CTAB)

Exactly what the Ag^+ ions from silver nitrate ($AgNO_3$) does in the growth solution of the synthesis is not yet known. However, the presence of the ions is essential. The presence of silver steers the selectivity for reduction on the nanorod tips and stabilises the lateral facets [16]. Thereby will the concentration of $AgNO_3$ affect the aspect ratio of the gold nanorods. Other species, CTA^+ cation and bromide, also influence the structure and shape directing of the growing nanorods. The species are believed to bind to distinct crystal facets which then influences the deposition rate of gold on the facets. For gold and other noble metals with face centered cubic (fcc) structures are the low-index {111} and {100} facets more thermodynamically stable compared to high-index facets [17]. The low-index facets is therefor favored during nanocrystal growth. However, the surface energies of the different facets can be changed by the interaction of ions and surfactants creating nanocrystals with different geometries enclosed by high-index facets. Gold nanorods synthesised from a seed-mediated method with the presence of CTAB and $AgNO_3$ are reported by Carbo-Argibay et al. [20] to have high-index surface facets such as {250} and {520}. High-index crystalline facets are also reported by Katz-Boon et al. [21] and predicted by density functional theory calculations by Almora-Barrios et al. [22].

2.2.2 Electrostatic Self Assembly of Gold Nanorods on Glass Substrates

Immobilising gold nanorods on glass substrates can be done with electrostatic self assembly. Gold nanorods synthesised from a seed-mediated method will have a surface charge due to the used capping agent. Often is hexadecyltrimethylammonium bromide (CTAB) used as the capping agent in the synthesis protocol [16]. CTAB forms a bilayer on the surface of the gold nanorods and the positive head group of CTAB gives the gold nanorods a positive surface charge. An illustration of electrostatic assembly of gold nanorods on a negatively charged glass surface is presented in Figure 2.2.

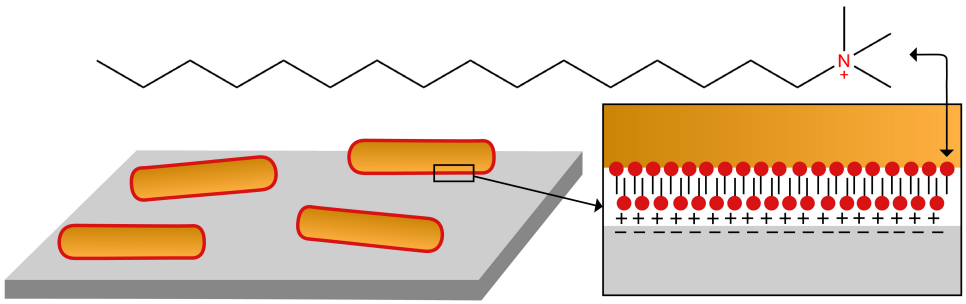

Figure 2.2: Illustration of electrostatic assembly of gold nanorods on a negatively charged glass surface

The surface of the glass substrates can be made negatively charged from chemical etching with nitric acid (HNO_3). Nitric acid cleans the glass surfaces and leaves them negatively charged due to leaching of ions from within the surface. Aluminum, calcium and sodium are effectively reduced from the glass surface with usage of nitric acid [23]. A drawback with utilising electrostatic assembly is that it may destabilise due to ionic strength if the surface is immersed in a solution.

2.2.3 Localised Surface Plasmon Resonance Frequency of Gold Nanorods

Localised surface plasmon resonance (LSPR) is a collective electron oscillation occurring in metallic nanoparticles that are excited by light. Plasmons can be stated as negatively charged electron clouds that are coherently displaced from their equilibrium positions around a lattice of positive ions [24]. Plasmon oscillation distributed over the total volume of a particle occurs when the particle is of nano-size and smaller than the photon wavelength. The plasmons in the nanoparticle are then referred to as localised surface plasmons (LSP). To be able to excite the LSP the incident light needs to have a frequency in resonance with the oscillation. With exposure to an electromagnetic wave of a relevant frequency, the metal nanoparticle conduction band electrons will sustain a collective coherent oscillation that is in resonance with

the frequency of the incident light [19]. Hence, localised surface plasmon resonance will occur.

Metal nanoparticles, such as gold nanorods, have strong absorption of incident light at specific frequencies due to the LSPR phenomena, which can be seen in an absorption spectrum. This is the reason for the strong color that colloidal metal nanoparticle solutions exhibit [19]. The strong absorption of incident light, the maximum of light extinction (sum of absorption and scattering), is occurring at the LSPR frequency. Gold nanospheres in an aqueous solution have a strong and broad LSPR absorption band at roughly 520 nm [5]. Gold nanorods split their LSPR into two distinct absorption bands, a transverse and a longitudinal band [15]. The transverse and longitudinal band corresponds to the short and the long axis of the rod respectively. The absorption bands of gold nanorods are illustrated in the Figure 2.3.

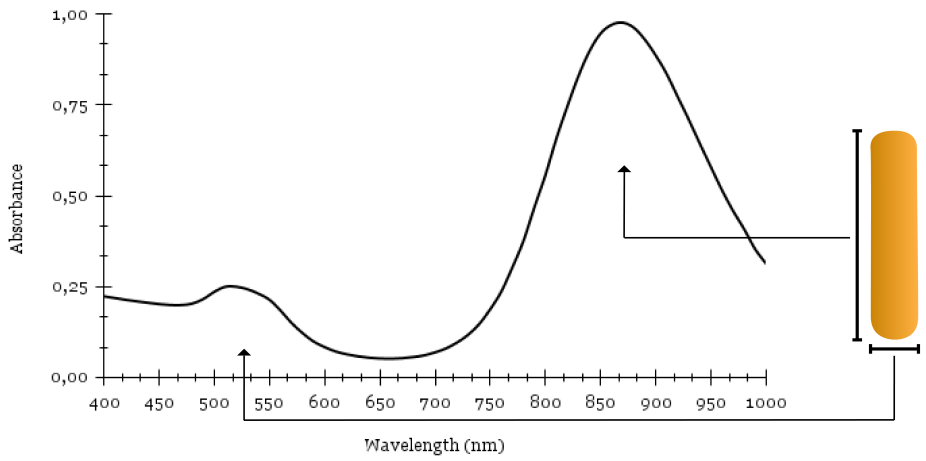

Figure 2.3: Transverse and longitudinal absorption bands illustrated in localised surface plasmon resonance spectrum of gold nanorods

The transverse absorption band of gold nanorods occurs in the visible region similar to gold nanospheres and is not very sensitive to the dimensions of the rods [19]. The longitudinal band can be tuned through the visible to near-infrared (NIR) region and the spectral position depends on the aspect ratio (length/width) of the rods [5]. The longitudinal surface plasmon resonance is hence controllable in the visible or NIR region, where an increase in aspect ratio causes a red-shift of the LSPR [25]. The surrounding medium also affects the surface plasmon resonance wavelength, an increase in refractive index leads to a red-shift of the wavelength [19].

As previously mentioned, when gold nanorods are irradiated with the light of their LSPR frequency, excitation of the conduction band electrons will occur, leading to

coherent oscillation of the electrons. However, once the excited conduction band electrons decay to the ground state their energy is released as heat to the surroundings. It therefore results in heating when gold nanorods are illuminated at their LSPR wavelength [5]. Due to this gold nanorods are attractive for application in the field of photothermal therapy, such as cancer treatment. Clinical applications are suitable for gold nanorods with LSPR in the NIR region since aqueous tissue barley absorbs light in the NIR window between approximately 700 and 1200 nm [5].

2.2.4 Toxicity of Gold Nanorods

It is of high importance to understand nanomaterial toxicity and the influence of size and shape when researching nanomaterials for biological applications. Not much is known considering long-term effects of nanomaterials on human health and environmental impact. Nanoparticles in aqueous solution often have a surface charge that through electrostatic repulsion stabilises them from aggregating. Biological media with electrolytes and high ionic strength can make the nanoparticles aggregate via electrostatic screening [26]. Once the nanoparticles aggregate their ability to interact with and enter cells can be changed.

Gold has a high electron density and is in bulk, one of the most chemically inert metals [5]. One possible risk with gold nanorods are distribution into organs including the central nervous system. Gold nanorods in the size range of 10-100 nm are more slowly taken up by cells compared to nanospheres in the same range [27], and gold nanoparticles bigger than 5 nm can be assumed to be chemically inert just like gold in its bulk form [28]. Even if gold nanorods in many cases are bigger than 5 nm the ligands attached to the surface of the nanorods may affect the toxicity. Therefore, the toxicity of the chemicals used in the synthesis is also needed to be assessed.

There are studies showing that gold nanoparticles themselves might not cause toxicity, but precursors from the synthesis may [29]. The capping agent hexadecyltrimethylammonium bromide (CTAB) used in the synthesis is highly toxic. CTAB molecules in solution and on the surface of the gold nanorods are identified as cytotoxic [30]. A problem left to solve is how to control the toxicity of CTAB in the preparation of the gold nanorods. CTAB can damage mitochondria and kill cells by entering them both with or without being attached on gold nanorods [30]. The toxicity can be reduced by purification of the nanorods, and by surface functionalisation of the gold nanorods to reduce the toxicity of residual CTAB. Different surface modifiers have been tested, however more efforts are needed to find a more simple, inexpensive and sustainable nontoxic modifier that also is worthier for clinical use [30]. It also is further interesting to evaluate the toxicity of the gold nanorods once they are immobilised on a surface.

3

Methodology

The methodology includes synthesis, purification, characterisation of gold nanorods, and gold nanorod surface assembly on glass substrates. The methodology also includes photothermal heating and characterisation of the material surfaces, tests for microbial exposure and evaluation with microbiological studies.

3.1 Materials

Milli-Q® (18.2 MΩcm, Millipore) water was used during the experiments of the project. The chemicals used for the gold nanorod synthesis were hexadecyltrimethylammonium bromide (≥98 %, Sigma-Aldrich), gold(III) chloride trihydrate (≥99.9 % trace metals basis, Sigma-Aldrich), sodium borohydride (99 % ReagentPlus® , Sigma-Aldrich), hydrochloric acid (≥37 %, Sigma-Aldrich), silver nitrate (≥99.9999 % trace metals basis, Sigma-Aldrich) and L-ascorbic acid (reagent grade, crystalline, Sigma-Aldrich). For preparation of gold nanorod-functionalised surfaces nitric acid (65-67 %, Sigma-Aldrich), ethanol (95.5 % analytical grade, Solveco) and ethanol (99.5 % analytical grade, Solveco) were used. Glassware and magnet stir bars used during the gold nanorod synthesis and preparation of the gold nanorod-functionalised surfaces were cleaned with a basic piranha solution. The basic piranha solution was prepared with Milli-Q water, ammonia solution (32 %, Merck) and hydrogen peroxide solution (>30 %, Fisher Scientific) in a 4:1:1 ratio. The cleaning was done by heating the basic piranha solution to 80 °C for at least 20 minutes and followed by thorough rinsing of the equipment with Milli-Q water.

For the microbiological studies trypticase soy agar (TSA) plates, brain heart infusion (BHI) agar plates, and *Staphylococcus aureus* (strain CCUG 10778) were used. The laser diode used for photothermal heating and *in vitro* studies was a K808DA5CN-55.00W from BWT BEIJING with output wavelength 808 nm ± 3 nm.

3.2 Synthesis and Purification of Gold Nanorods

The synthesis of gold nanorods follows a procedure modified from a method described in the supporting information of the article by Scarabelli et al. [16]. The modifications made in the synthesis method were changes in concentrations for the

stock solutions of silver nitrate ($AgNO_3$) and L-ascorbic acid dispersed in Milli-Q water. These changes were applied in order to tune the aspect ratio of the gold nanorods, and thus also the localised surface plasmon resonance (LSPR) frequency. Since it is of interest to evaluate the bacterial elimination of the surfaces with bacterial contamination from air, the photothermal heating needed to occur in air. For the evaluation of the antimicrobial activity of the gold nanorod-functionalised surfaces, the surfaces were irradiated with near-infrared light at 808 nm. Therefore, the gold nanorods needed to be tuned, in order to have a LSPR frequency in air that is in the spectral region of the laser.

3.2.1 Synthesis of Gold Nanorods

The synthesis started with the preparation of a seed solution. The synthesis of the seed solution was performed in a water bath at 30 °C. A volume of 25 µL of gold(III) chloride trihydrate ($HAuCl_4 \cdot 3H_2O$, 50 mM) was added to 4.7 mL hexadecyltrimethylammonium bromide (CTAB, 0.1 M) and the mixture was slowly stirred for 5 minutes. 300 µL of a newly prepared sodium borohydride solution ($NaBH_4$, 10 mM) was then added under strong stirring at 1400 rpm. Then after approximately 20 seconds was the mixture mildly stirred at 400 rpm. The light brown seed solution was kept mildly stirred and in a water bath at 30 °C until use.

The growth of single crystal nanorods was preformed in a water bath at 30 °C. A volume of 190 µL of hydrochloric acid (HCl, 1 M) and 100 µL of $HAuCl_4$ solution (50 mM) was added to 10 mL of CTAB (0.1 M), and the mixture was gently stirred for 5 minutes. Afterwards, 120 µL of silver nitrate solution ($AgNO_3$, 11 mM) was added to the mixture, and it was then gently shaken for a few seconds. 100 µL L-ascorbic acid solution (90 mM) was added and the mixture was thoroughly shaken and turned colorless from a previously yellow color. Finally, 24 µL of the seed solution was added to the mixture and it was strongly shaken by hand. The growth solution was then left undisturbed at 30 °C for 2 hours. This synthesis procedure of gold nanorods was scaled up 6 times the original volumes.

3.2.2 Purification of Gold Nanorods

Centrifugation was used to purify the synthesised gold nanorods. The gold nanorod dispersion was centrifuged at 1800 xg at 28 °C for 45 minutes. Afterwards the supernatant was removed and the precipitate, the gold nanorods, was re-dispersed in Milli-Q water. The centrifugation and re-dispersion was preformed totally three times. After the last centrifugation the gold nanorods were re-dispersed in Milli-Q water again and stored in 4-5 °C protected from sunlight.

3.3 Surface Assembly of Gold Nanorods

Two sizes of glass substrates, large and small, was used for the gold nanorod surface assembly. The large substrates were microscope slides from Epredia cut in half to a size of 38 · 26 mm. The small substrates were round with a diameter of 13 mm

from VWR®. All glass substrates were cleaned with ethanol 95% followed by Milli-Q water and dried with nitrogen gas. The substrates were then left in nitric acid 65-67 % for approximately 20-24 h and then rinsed with Milli-Q water. 1.5 mL of a 0.2 nM gold nanorod dispersion in Milli-Q were added on the large glass substrate surfaces. The large substrates were placed in a petri dish inside a desiccator cabinet with approximately 85-95 % relative humidity for 4 h. The small glass substrates were immersed in 500 µL of 0.2 nM gold nanorod dispersion for 4 h. The gold nanorod dispersion was then stepwise exchanged into Milli-Q water and finally the nanorod-functionalised surfaces were drenched in ethanol 99.5 % and then air dried.

The concentration of the gold nanorod dispersion used for the gold nanorod surface assembly was calculated from absorbance values obtained from UV-Vis-NIR spectrum. These calculations were compared to theoretical concentration calculations. Example calculations, based on absorbance values and theoretical calculations, are presented in Appendix AI and AII.

3.4 Photothermal Heating of Gold Nanorods Immobilised on Glass

The photothermal heating of the gold nanorod-functionalised glass surfaces was measured by irradiating the surfaces with a near-infrared (NIR) laser at 808 nm and measuring the temperature before and after the irradiation with an infrared thermometer gun. The laser was used both at 10 W and 15 W. The large substrates were used for the measurements. A programmable xy-plotter robot was used for even irradiation of the whole surface. The xy-plotter was programmed in the Universal Gcode Sender to irradiate the whole surface by moving at a speed of 90 mm/min. As a reference, bare glass surfaces were also irradiated and the temperature change was measured. Three replicates of each type of surface were used for 10 W. However, six replicates of each type of surface were analysed for 15 W.

3.5 *In Vitro* Studies of Photothermal Elimination

Two *in vitro* studies were performed to evaluate how well gold nanorod-functionalised surfaces can eliminate microbiological contamination. One *in vitro* studie exposed surfaces in laboratory rooms and the other utilised growth of *Staphylococcus aureus* (*S. aureus*) on the surfaces.

3.5.1 Microbial Contamination From Surface Exposure in Laboratory Room

The large sized substrates were used for the exposure experiments. Samples of gold nanorod-functionalised surfaces and bare glass substrates were exposed in the laboratory room environment for 5 days. The surfaces were placed in a large petri dish open to the surroundings on a lab bench. Before exposure the bare glass

substrates were cleaned with ethanol 95 %, followed by Milli-Q water and then drenched in ethanol 99.5 % and dried. A NIR laser (808 nm) was used at 10 W and 15 W, in the same way described in Section 3.4. Four different groups were used for this microbiological study with at least three replicates of each group.

1. Gold nanorod-functionalised glass irradiated with NIR light (AuNR-Glass + NIR)

2. Gold nanorod-functionalised glass (AuNR-Glass)

3. Glass irradiated with NIR light (Glass + NIR)

4. Glass (Glass)

Both the irradiated surface samples and the non-irradiated samples were placed with the exposed side of the surface against trypticase soy agar (TSA) or brain heart infusion (BHI) agar plates. The surfaces were gently pressed against the agar plates and then left undisturbed. After 10 minutes the surfaces were removed and the agar plates were incubated at 37 °C. Colony-forming unit (CFU) was then used as an evaluation method and CFU counting was done after 24 and 48 h.

3.5.2 Bacteria Cultured on Gold Nanorod-Functionalised Glass

Microbiological studies with growth of *Staphylococcus aureus* (*S. aureus*) on gold nanorod-functionalised glass surfaces was conducted to evaluate the antimicrobial activity of the surfaces achieved upon irradiation with NIR light. The small sized gold nanorod-functionalised glass substrates were used for this experiment. Three different groups were applied to this microbiological study with triplicates of each group.

1. Gold nanorod-functionalised glass (AuNR-Glass)

2. Gold nanorod-functionalised glass irradiated with NIR light (AuNR-Glass + NIR)

3. Gold nanorod-functionalised glass with LSPR frequency at 742 nm in air irradiated with NIR light (AuNR-Glass^{742} + NIR)

The substrates called AuNR-Glass^{742} were produced during previous work within the research group. These substrates were made following the same method as in Section 3.2 and surface assembly as in Section 3.3. However, the synthesis of the gold nanorods differed, producing nanorods with a different aspect ratio. Therefore, the substrates have gold nanorods with different dimensions compared to the gold nanorods synthesised for this project. The gold nanorods on the AuNR-Glass^{742} surfaces were produced to have a localised surface plasmon resonance (LSPR) frequency

close to 808 nm when irradiated in water, and they have an LSPR frequency at approximately 742 nm when irradiated in air on a glass surface. More characteristics of the AuNR-Glass^{742} substrates are presented in Appendix AIII.

S. aureus (CCUG 10778) were cultured on brain heart infusion agar at 37 °C for approximately 16 h. One colony was then dispersed into 4 mL of tryptic soy broth (TBS) and incubated at 37 °C for 3 h until a mid-log phase of OD 0.6 was achieved. The bacterial suspension was then diluted with phosphate-buffered saline (PBS) with glucose to a concentration of $1.2 \cdot 10^8$ CFU/mL. The final bacterial suspension contained 12 % TSB and 88 % PBS with glucose.

All surface substrates used for the experiment were sterilised by immersion in 70 % EtOH for 15 min, rinsed with sterile water and placed in a 24-well plate. The prepared bacterial suspension was added to the wells and the substrates were incubated at 37 °C. After 2.5 h, the substrates were rinsed four times in PBS with glucose and placed on microscope slides to dry. After approximately 5 minutes of drying the substrates from group 2 and 3 were irradiated with NIR light (808 nm) at 15 W for 5 seconds. All substrates were then stained with 10 µL of LIVE/DEAD™ BacLight™ (ThermoFisher Scientific). The samples were then studied with a fluorescence microscope.

3.6 Analytical Techniques and Characterisation

Analytical techniques such as UV-Vis-NIR spectroscopy, scanning electron microscopy (SEM) and fluorescence microscopy were used for characterisation and evaluation. This section presents the techniques and the grounds for usage of them.

3.6.1 UV-Vis-NIR Spectroscopy

Spectroscopy with light in the ultraviolet, visible and near-infrared region of the electromagnetic spectrum is called UV-Vis-NIR spectroscopy. The wavelength range for each region are approximately 180-380 nm, 380-700 nm and 700-2500 nm for UV, visible and NIR light respectively. By sending monochromatic photons through a specimen, measuring the transmitted light and comparing it to a reference cuvette, a spectrophotometer plots the absorbance as a function of wavelength [31]. The absorbance is related to the concentration of the specimen which is described by Beer-Lamberts law in Equation 3.1,

$$A = log(\frac{I_0}{I}) = \epsilon * C * l \tag{3.1}$$

where A is the absorbance, l is the path length, C is the concentration, ϵ is the molar extinction coefficient, I_0 is the intensity measured through a reference cuvette and I is the intensity of the light transmitted thought the specimen [31].

Characterisation with UV-Vis-NIR spectroscopy of the synthesised gold nanorods dispersed in Milli-Q water and of the gold nanorod-functionalised glass surfaces was carried out to obtain the LSPR spectra of the samples. The instrument used for UV-Vis-NIR measurements of gold nanorods dispersed in Milli-Q water was a Thermo Scientific™ Multiskan™ GO spectrophotometer with a wavelength range from 200 nm to 1000 nm. For UV-Vis-NIR measurements of gold nanorod-functionalised glass surfaces in air an Agilent 8453 UV-visible Spectroscopy System with a wavelength range from 190 nm to 1100 nm was used.

The concentration of gold nanorods dispersed in Milli-Q water was derived from the absorbance spectra. The absorbance at 400 nm has an equal contribution from gold nanoparticles with the same volume, since the main absorbance contribution is related to interband transitions in gold [16]. An absorbance value of 1.2 at 400 nm corresponds to a concentration of 0.5 mM of Au(0). This allows the concentration of Au(0) to be calculated by Equation 3.2,

$$[Au(0)] = \frac{A_{400}}{1.2} * 0.5 * 10^{-3} \tag{3.2}$$

where A_{400} is the absorbance at 400 nm [16]. The calculations of the concentration of the gold nanorod dispersion obtained from the absorbance in UV-Vis-NIR spectrum was compared to theoretical concentration calculations. Example calculations, based on absorbance values and theoretical calculations, are presented in Appendix AI and AII.

3.6.2 Scanning Electron Microscopy

Morphological, chemical and structural information from the surface of a specimen, at high resolution, can be attained by usage of a scanning electron microscope (SEM). SEM uses electromagnetic lenses to focus and scan an electron beam over the surface [31]. Condenser and objective lenses are used to demagnifying the current crossover of the electron gun to produce a small electron probe at the specimen surface. The electron source, electron gun, can be thermionic, field-emission or Schottky source. The electron beam's interaction with the surface generates energy emissions, such as secondary and backscattered electrons, that then are detected by various detectors and the signals are converted into an image [31]. The image resolution can be achieved down to nanometer scale.

Secondary electron imaging provides topographical contrast. The secondary electrons are a result of inelastic interactions between the electron beam and the sample, and they originate from the surface region of the specimen sample. Backscattered electron imaging provides information on the composition of the specimen due to high sensitivity to differences in atomic number [31]. Backscattered electrons come from deeper regions of the sample and are reflected after elastic interactions between the sample and the electron beam.

SEM was used together with image analysis of SEM micrographs to obtain the dimensions and the surface coverage of the synthesised gold nanorods. The SEM used was Zeiss Ultra 55 with a field emission gun. The image analysis program used was Fiji (ImageJ, National Institute of Health, USA) and the gold nanorods were approximated as rectangles in the image analysis.

3.6.3 Fluorescence Microscopy

Fluorescence microscopy is an imaging technique often used to observe the localisation of molecules within cells. The technique uses the excitation of fluorophores in a specimen and subsequent detection of the fluorescence signal to generate an image. The analysed specimen is illuminated with usually blue or ultraviolet light and then analysed through a barrier filter [32]. The fluorophores in the specimen absorb light and then emit light of a longer wavelength. The filter is sorting out the exciting light without blocking the emitted fluorescence, making it possible to visualise the fluorescent objects in the specimen [33]. The specimen used for fluorescence microscopy needs to contain fluorophores, either being autofluorescence or stained with fluorescent probes.

Fluorescence microscopy was used together with the image analysis program Fiji (ImageJ, National Institute of Health, USA) to evaluate the amount of eliminated bacteria after irradiation with NIR light in the *in vitro* studies with growth of *Staphylococcus aureus* on the surfaces. The microscope used was an Axio Imager Z2m microscope (Zeiss) equipped with an HBO-lamp for fluorescence imaging. The samples were stained with LIVE/DEAD™ BacLight™ (ThermoFisher Scientific), that contains both a green- and red-fluorescent nucleic acid stain. The green-fluorescent stain penetrates all cells and the red-fluorescent stain only penetrates cells with damaged membranes (dead cells).

4

Results and Discussion

Results achieved are presented and discussed in this chapter. Characterisation of the gold nanorods are presented for gold nanorods in aqueous dispersion and immobilised on glass surfaces. Following this, results from the two *in vitro* studies are presented and discussed.

4.1 Characterisation of Gold Nanorods

This section will present results from the characterisation of the gold nanorods synthesised from the seed-mediated method. The LSPR spectra will be shown for both gold nanorods in aqueous dispersion and the gold nanorod-functionalised surfaces. This will be followed by a presentation of dimensions of gold nanorods, surface coverage and photothermal heating of gold nanorod-functionalised glass surfaces.

4.1.1 Localised Surface Plasmon Resonance Spectra of Gold Nanorods in Aqueous Dispersion and Immobilised on Glass

The gold nanorods dispersed in Milli-Q water showed a LSPR spectrum with a transverse absorption band at 505-525 nm and a longitudinal band at 850-890 nm, with a peak at 870 nm. Measured in the air, the gold nanorod-functionalised surfaces exhibited a LSPR spectrum with a transverse absorption band at 515-535 nm and a longitudinal band at 775-815 nm, with a peak at 795 nm. An example spectra is presented in Figure 4.1. The spectral data is normalised for both gold nanorod-functionalised glass (AuNR-Glass) and gold nanorods in Milli-Q water (AuNR). A shift occurs of approximately 75 nm when the gold nanorods are measured in air immobilised on glass compared to free in water. This is due to change of refractive index. The spectral output (808 nm) of the NIR laser used in this project is in the range of the longitudinal absorption band of the gold nanorod-functionalised glass surfaces (775-815 nm). Hence, the gold nanorod-functionalised glass surfaces should generate heat when illuminated by the NIR laser in the air.

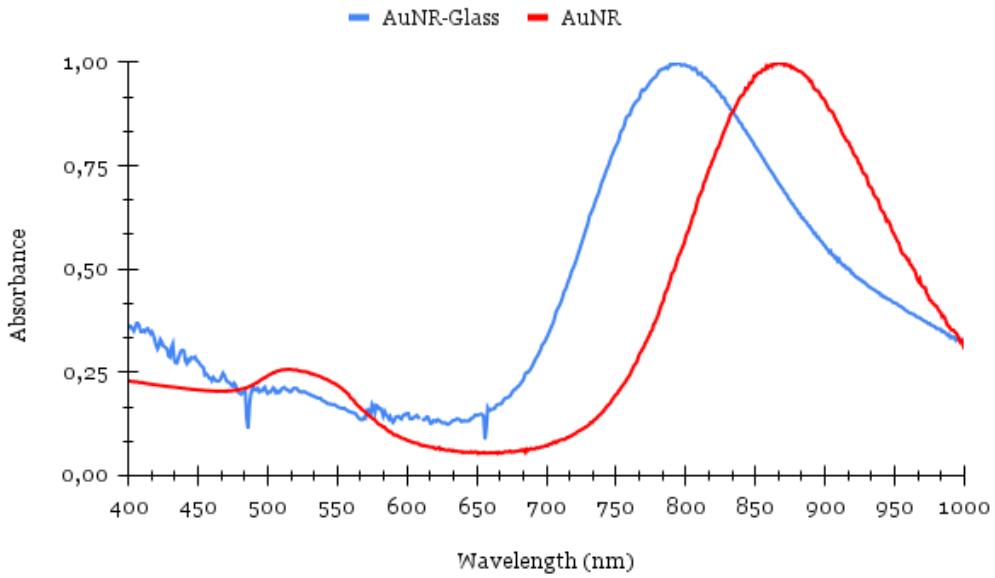

Figure 4.1: Localised surface plasmon resonance spectra of gold nanorod-functionalised glass measured in air (AuNR-Glass) and gold nanorods dispersed in Milli-Q water (AuNR)

4.1.2 Dimensions of Gold Nanorods

Length, width and aspect ratio of the gold nanorods are presented in Table 4.1. The mean values of the gold nanorods' length, width and aspect ratio are 68 nm, 18 nm and 3.9 respectively. For the image analysis determining the nanorods' dimensions, a total of 5045 nanorods were analysed.

Table 4.1: Length, width and aspect ratio of gold nanorods with standard deviation

Length (nm)	Width (nm)	Aspect ratio (Length/Width)
68.32 ± 9.49	18.21 ± 4.21	3.93 ± 0.97

4.1.3 Surface Coverage of Gold Nanorods Immobilised on Glass

Two sizes of glass substrates, large and small, were used in the project to produce the gold nanorod-functionalised surfaces. An even coverage of gold nanorods was shown using scanning electron microscopy (SEM) to evaluate the functionalised surfaces. The gold nanorods were randomly orientated and did not form any larger aggregates. However, some gold nanospheres were present. Representative SEM micrographs in Figure 4.2 show gold nanorods on glass substrates with a 50 000x magnification.

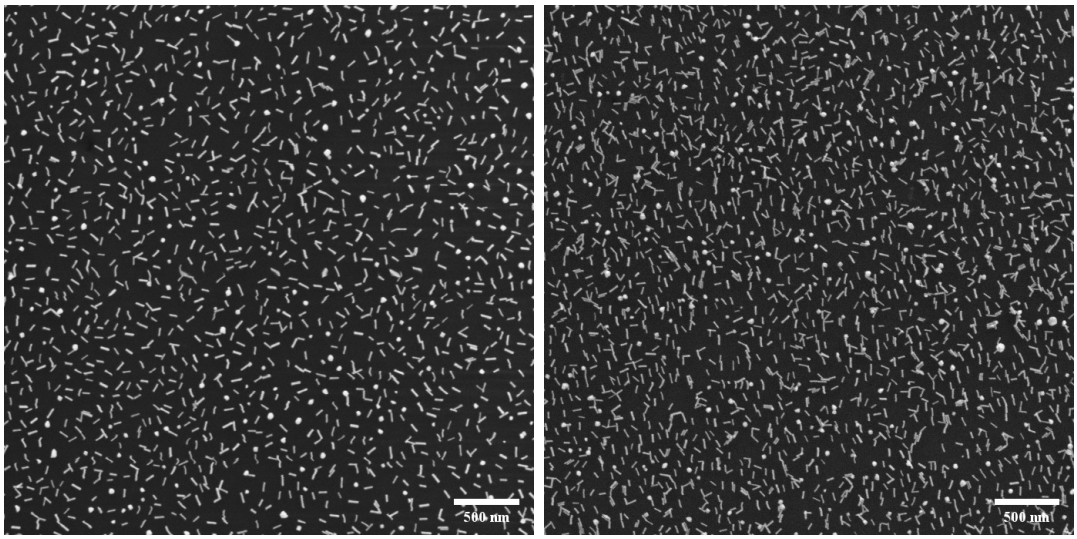

(a) Large substrate **(b)** Small substrate

Figure 4.2: Scanning electron microscopy micrographs of gold nanorod-functionalised glass at 50 000x magnification, shown for both large (a) and small (b) substrates

The surface coverage of the gold nanorods was determined by image analysis of SEM micrographs and is presented in Table 4.2. The average surface coverage was 11 % which corresponds to 88 nanorods/µm^2 for the large glass surfaces. The average surface coverage for the small glass surfaces was 13 % which corresponds to 107 nanorods/µm^2. In total 45 different SEM micrographs were used for the analysis of both the large and the small glass surfaces.

Table 4.2: Average surface coverage with standard deviation for both large and small surfaces

Surface	**Average Surface Coverage**	
	%	**nanorods/µm^2**
Large	10.9 ± 1.4	88.4 ± 10.9
Small	13.3 ± 1.2	106.7 ± 9.8

There was a significant difference in surface coverage for the large and the small surfaces on a 95 % significance level, despite the samples being prepared in an equivalent way. The difference in surface coverage is probably due to that the glass substrates are produced by different manufacturers and therefore have differences in chemical composition.

4.1.4 Photothermal Heating of Gold Nanorods Immobilised on Glass

The photothermal heating of gold nanorod-functionalised glass surfaces was evaluated by measuring the temperature increase when the surfaces were irradiated with NIR light with two different powers, 10 W and 15 W. Both gold nanorod-functionalised glass (AuNR-Glass) and bare glass (Glass) was used for the evaluation. The average temperature increase is presented in Table 4.3. For the glass surfaces the average temperature increase was 1 °C and 1.5 °C for 10 W and 15 W respectively. The nanorod-functionalised glass showed a temperature increase of 10.4 °C for 10 W and 15.8 °C for 15 W. The average temperature increase was significantly different for Glass compared to AuNR-Glass on a 95 % significance level. The gold nanorods increased the temperature of the surrounding air with 9-14 °C compared to the control, and the temperature increase was higher for higher power of the laser. The temperature increase measured for the gold nanorod-functionalised surfaces shows the photothermal heating achieved due to LSPR. The variations in the temperature increase are likely caused by delay between irradiating the surface and measuring the temperature.

Table 4.3: Average temperature increase with standard deviation for gold nanorod-functionalised glass (AuNR-Glass) and bare glass (Glass) after irradiation with near-infrared light at 10 W and 15 W

Surface	**Δ T (°C)**	
	10 W	**15 W**
Glass	1.0 ± 0.3	1.5 ± 0.4
AuNR-Glass	10.4 ± 1.3	15.8 ± 2.9

4.2 *In Vitro* Studies of Photothermal Elimination

Results from the *in vitro* studies of this project are presented in this section. First, the results from the study on exposed gold nanorod-functionalised glass surfaces in laboratory rooms are presented and discussed. This is followed by the results from the study performed with *Staphylococcus aureus* (*S. aureus*) cultured on gold nanorod-functionalised glass surfaces.

4.2.1 Microbial Contamination From Surface Exposure in Laboratory Room

Two different trials were made for surfaces exposed in a laboratory room for 5 days. The first trial used irradiation with NIR light at 10 W, and the second trial used NIR light at 15 W. Both trials used an irradiation speed of 90 mm/min and included four groups, consisting of two types of surfaces and two types of treatments. Each group had at least three replicates. The surfaces tested were gold nanorod-functionalised

glass (AuNR-Glass) and bare glass (Glass). The treatment was either irradiation with NIR light (+ NIR) or no irradiation. The AuNR-Glass surfaces had an average surface coverage of 11 % corresponding to 88 nanorods/µm^2. Colony-forming unit (CFU) was counted for each replicate after both 24 and 48 hours. Example pictures of agar plates with colonies are presented in Appendix BI in Figure B1

The statistical significance of the results was evaluated using paired samples t-test as well as a 2^2 factorial design. The paired samples t-test compared population means of the groups Glass and AuNR-Glass, Glass and Glass + NIR, and AuNR-Glass and AuNR-Glass + NIR. The 2^2 factorial design studied the effect of each factor, surface type (Glass or AuNR-Glass) and treatment (no-NIR or NIR), on the response (CFU), as well as the effects of interactions between factors on the response. Example of statistical calculations with the 2^2 factorial design is presented in Appendix BIII.

4.2.1.1 Results Using Near-Infrared Light Irradiation at 10 W

The average number of CFU with standard deviation counted after 24 and 48 h for the trial using NIR light at 10 W is presented in Table 4.4 below. The number of CFU counted for each replicate is presented in Appendix BI in Table B1.

Table 4.4: The average number of colony-forming unit with standard deviation for bare glass surfaces (Glass) and gold nanorod-functionalised glass surfaces (AuNR-Glass), either non-irradiated or irradiated with 10 W at 808 nm (+ NIR)

Surface	**CFU**	
	24 h	**48 h**
Glass	4.7 ± 1.5	7.0 ± 2.6
AuNR-Glass	5.0 ± 3.0	12.7 ± 5.9
Glass + NIR	4.3 ± 1.5	6.3 ± 1.5
AuNR-Glass + NIR	7.7 ± 3.2	9.7 ± 3.1

P-values of the t-tests are presented for this trial in Appendix BII in Table B3. The paired t-test showed no significant difference between the groups. Using the 2^2 factorial design to evaluate the data gave more insight. The analysis of variance (ANOVA) tables for for both CFU counted after 24 h and 48 h are presented in Appendix BIV in Table B7 and B8.

The 2^2 factorial design showed that there were no significant factors (surface type, treatment and interaction) after 24 h at a 90 % significance level. However, after 48 h the type of surface (Glass or AuNR-Glass) was significant at a 90 % significance level. At this level a surface with gold nanorods was more likely to exhibit a higher CFU compared to a bare glass surface, independent of treatment (no-NIR or NIR). The reason why a surface with gold nanorods showed more CFU can be due to that airborne particles and bacterial cell surfaces have a net negative surface charge [34] and are therefore attracted to the positively charged nanorods on the surface.

The combination of gold nanorods and NIR light did not show any antimicrobial activity in this trial. One possible explanation could be that the power of the laser was too low or the irradiation time too short. Bacteria travel in the air on particles and once these particles land on the surface the bacteria may not be in direct contact with the gold nanorods. The heat from the gold nanorods must then conduct though the particles to reach the bacteria, which could be another explanation as to why no antimicrobial activity was detected.

4.2.1.2 Results Using Near-Infrared Light Irradiation at 15 W

Since no significant antimicrobial activity was observed for the interaction of gold nanorods and NIR light in the first trial, the power of the NIR laser was increased with 50 % for the second trial. To further increase the reliability of the results, 6 replicates were used. The average number of CFU with standard deviation counted after 24 and 48 h for the trial using NIR light at 15 W is presented in Table 4.5 below. The number of CFU counted for each replicate is presented in Appendix BI in Table B2.

Table 4.5: The average number of colony-forming unit with standard deviation for bare glass surfaces (Glass) and gold nanorod-functionalised glass surfaces (AuNR-Glass), either non-irradiated or irradiated with 15 W at 808 nm (+ NIR)

Surface	**CFU**	
	24 h	**48 h**
Glass	7.8 ± 3.4	9.2 ± 3.3
AuNR-Glass	13.0 ± 8.3	16.2 ± 9.0
Glass + NIR	12.0 ± 7.1	15.3 ± 7.4
AuNR-Glass + NIR	8.8 ± 3.0	11.5 ± 3.2

P-values of the t-tests for this trial are presented in Appendix BII in Table B4. There was no significant difference among population means between the groups at a 95 % significance level. The same was true for a 90 % significance level for all groups, except for Glass compared to Glass + NIR with CFU counted after 48 h. The mean value was higher for the Glass + NIR surfaces compared to the Glass surfaces, meaning that a bare glass surface irradiated with NIR light would show more CFU compared to a non-irradiated glass surface. The temperature was mildly increased when the glass surfaces were irradiated with NIR light. This temperature increase may have made the climate more favourable for the bacteria, so a higher amount of bacteria survived during the trial procedure, compared to the non-irradiated glass surfaces.

The p-value for the comparison of Glass and AuNR-Glass for CFU counted after 48 h was 0.1020. This almost indicate a significant difference among population means for a 90 % significance level. The mean value was higher for the AuNR-Glass surfaces compared to the Glass surfaces, meaning that a non-irradiated glass surface with

gold nanorods would show more CFU compared to a non-irradiated glass surface. A similar correlation was shown in the 2^2 factorial design made for the trial using NIR light at 10 W with CFU counted after 48 h presented in Section 4.2.1.1. This correlation was probably mainly due to electrostatic attraction between the gold nanorods and the airborne microbes.

Analysis of variance (ANOVA) tables for both CFU counted after 24 h and 48 h, from the 2^2 factorial design, are presented in Appendix BIV in Table B9 and B10. The 2^2 factorial design showed that there were no significant factors (surface type, treatment and interaction) after 24 h at a 95 % significance level. However, after 48 h the interaction groups, Glass and AuNR-Glass + NIR, had a significantly lower number of CFU compared to the other groups at a 95 % significance level. Meaning that both the Glass surfaces and the AuNR-Glass + NIR surfaces are more likely to show fewer CFU compared to the other groups. The t-tests also indicated a lower CFU for the Glass surfaces compared to the Glass + NIR surfaces and AuNR-Glass. From the results of the t-test, the combination of NIR light and gold nanorods is expected to increase the CFU if the surface type and treatment are independent from each other. The combination has however been shown in the 2^2 factorial design to be significant, the AuNR-Glass + NIR surface group demonstrates a decreased CFU and that the surface type and treatment are dependent. This means that surfaces with gold nanorods treated with NIR light exhibit a reduction in CFU and that an antimicrobial activity was achieved. The Glass surfaces also demonstrated a decrease of CFU. This decrease is probably due to a lower probability for bacteria to deposit on the surfaces compared to a surface with gold nanorods, due to the previously discussed electrostatic attraction of particles and bacteria to gold nanorods.

Only a certain surface coverage and a certain power of the NIR light were evaluated in the project. There might be a combination of surface coverage and power that shows a more efficient antimicrobial activity. Therefore, it would be interesting for future work to find an optimum of antimicrobial activity by varying the surface coverage and power of the laser, especially towards higher values. Furthermore it would be interesting to expose the gold nanorod-functionalised surfaces in operating rooms for implants, to evaluate the elimination of the microbial contamination occurring in a clinical environment.

4.2.2 Bacteria Cultured on Gold Nanorod-Functionalised Glass

Two types of the small gold nanorod-functionalised glass surfaces were used in the *in vitro* study with culturing of *Staphylococcus aureus* to evaluate the antimicrobial activity of the surfaces upon NIR irradiation. Gold nanorod-functionalised glass with a LSPR frequency in air at 795 nm (AuNR-Glass) and gold nanorod-functionalised glass with a LSPR frequency in air at 742 nm (AuNR-Glass^{742}) were used in this study. The average surface coverage for the AuNR-Glass and the AuNR-Glass^{742} surfaces were 107 nanorods/µm^2 and 104 nanorods/µm^2 respectively. More characteristics for the AuNR-Glass^{742} surfaces are presented in Appendix AIII.

Three different surface groups were analysed in the study. AuNR-Glass, AuNR-Glass irradiated with NIR light at 15 W for 5 seconds (AuNR-Glass + NIR) and AuNR-Glass^{742} irradiated with NIR light at 15 W for 5 seconds (AuNR-Glass^{742} + NIR). The amount of dead (red) and live (green) bacteria was determined with fluorescence microscopy and subsequent image analysis. Representative images from the fluorescence microscopy are presented in Figure 4.3.

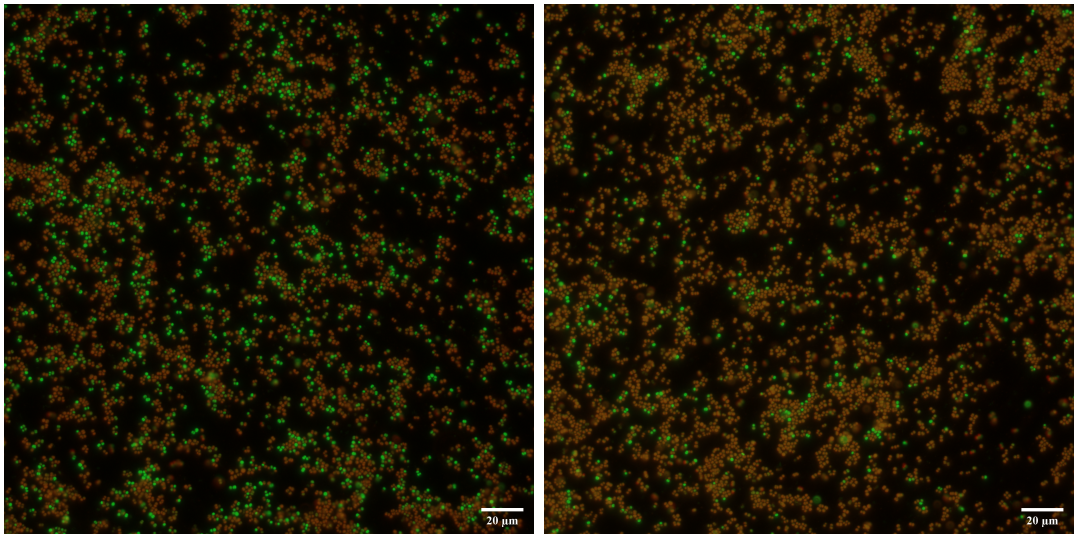

(a) AuNR-Glass **(b)** AuNR-Glass + NIR

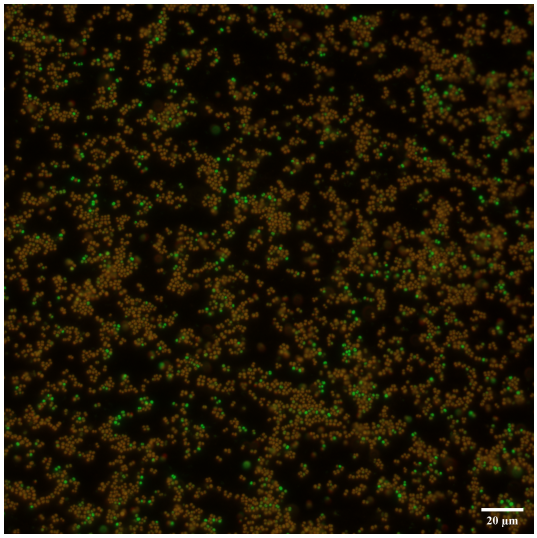

(c) AuNR-Glass^{742} + NIR

Figure 4.3: Images from fluorescence microscopy with a 40x magnification of samples stained with LIVE/DEAD™ from the *in vitro* study with *Staphylococcus aureus* cultured on gold nanorod-functionalised glass

The average percentage of dead bacteria for each surface group is presented in Figure 4.4 below. Each group had three replicates, and for each replicate 4 fluorescence images were analysed. The image analysis determined the area covered by dead (red) and live (green) cells. The average percentages of dead bacteria were 69 %, 84 % and 84 % for AuNR-Glass, AuNR-Glass + NIR and AuNR-Glass^{742} + NIR respectively. Determined with a paired samples t-test, the groups with NIR irradiation both had significantly different population means compared to the non-irradiated group on a 95 % significance level. The two NIR irradiated groups were however not shown significantly different from each other. P-values of the t-tests are presented in Appendix BV in Table B11.

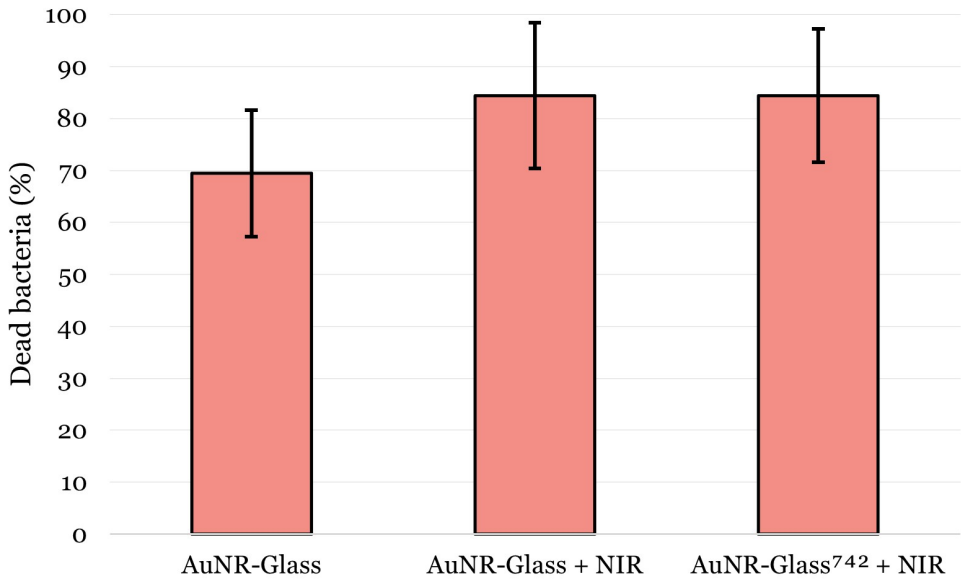

Figure 4.4: Percentage and standard deviation of dead bacteria covering the surfaces from the *in vitro* study with *Staphylococcus aureus* cultured on gold nanorod-functionalised glass

The two different gold nanorod-functionalised glass surfaces irradiated with NIR light both had a higher amount of dead bacteria, approximately 22 % more, compared to the non-irradiated surfaces. This indicates that a photothermal elimination of bacteria occurs due to the LSPR-produced heat from the gold nanorods. To improve the antimicrobial activity and photothermal elimination, the surface coverage of the gold nanorods could be increased, to increase the amount of gold nanorods in contact with bacteria.

The reason for the high amount of dead bacteria on the non-irradiated surfaces are probably due to the drying step in the procedure. Bacteria need a certain amount of water to survive and the drying time may have been too long for many of the bacteria and therefore killing them.

The different gold nanorod-functionalised glass surfaces had different LSPR frequencies and were irradiated at 808 nm in air, covered in bacteria. Since there was no significant difference between the two gold nanorod-functionalised surfaces the NIR light of 808 nm worked equally well regardless of the differences of the gold nanorods' dimensions and LSPR frequencies. The medium surrounding the surfaces during irradiation was air. However, the bacteria cultured on the surfaces were in contact with the gold nanorods. This means that some of the gold nanorods may have been in contact with a higher share of water than air, and the other way around, since the bacterial cells mainly consist of water. The refractive index surrounding each gold nanorod is therefore hard to estimate, but for the nanorods in contact with bacteria (i.e. water) a red-shift of the LSPR frequency likely occurred. If this change in refractive index made a big difference on the results is hard to know since the longitudinal band of the LSPR frequency is quite broad, covering 808 nm for both surface types, measured both in water and in air. Still, the variations in refractive index across the surfaces due to the presence of both bacteria and air can be part of the explanation why both types of gold nanorod-functionalised surfaces showed an antimicrobial activity.

5

Conclusion

Photothermal elimination of bacteria, both cultured and deposited from the surrounding environment on gold nanorod-functionalised glass surfaces, can be achieved with NIR light of the nanorods' LSPR frequency. The local heating from the photothermal effect was measured upon irradiation of gold nanorod-functionalised glass surface with NIR light and a temperature increase was detected. A procedure for the surface assembly of gold nanorods on glass, was established in the project. Two sizes of glass substrates were functionalised, where the large gold nanorod-functionalised glass surfaces exhibited a lower surface coverage of nanorods compared to the small gold nanorod-functionalised glass surfaces. The difference in surface coverage was attributed to differences in surface chemistry between the glass substrates.

The results from the *in vitro* study with microbial contamination from the laboratory room indicates an antimicrobial activity for the gold nanorod-functionalised glass surfaces irradiated with NIR light at 15 W. It also indicates that a surface with gold nanorods attracts more particles and bacteria from the surrounding environment, likely due to the electrostatic charge of the nanorods compared to a glass surface. From the *in vitro* study with *Staphylococcus aureus* cultured and partly dried on gold nanorod-functionalised glass surfaces an antimicrobial activity was observed for the surfaces irradiated with NIR light. Approximately 22 % more dead bacteria were present on the surfaces irradiated with NIR light compared to the non-irradiated control. A bigger effect could probably be achieved if the surface coverage of gold nanorods was higher, so more nanorods would be in contact with each bacteria.

From both the *in vitro* studies the results indicate that gold nanorods immobilised on a surface, which is irradiated with NIR light can photothermally eliminate bacteria located on the surface. Hence, the concept of utilising gold nanorod-functionalised substrates in combination with NIR light to help fight and prevent implant-associated infections shows promise for future work.

Bibliography

[1] Davide Campoccia, Lucio Montanaro, and Carla Renata Arciola. "The significance of infection related to orthopedic devices and issues of antibiotic resistance". In: *Biomaterials* 27.11 (2006), pp. 2331–2339. ISSN: 0142-9612. DOI: 10.1016/j.biomaterials.2005.11.044.

[2] Carla Renata Arciola, Davide Campoccia, and Lucio Montanaro. "Implant infections: adhesion, biofilm formation and immune evasion". In: *Nature Reviews Microbiology* 16.7 (2018), pp. 397–409. ISSN: 1740-1534. DOI: 10.1038/s41579-018-0019-y.

[3] Oliveira W.F. et al. "Staphylococcus aureus and Staphylococcus epidermidis infections on implants". In: *Journal of Hospital Infection* 98.2 (2018), pp. 111–117. ISSN: 0195-6701. DOI: 10.1016/j.jhin.2017.11.008.

[4] Maria Pihl, Ellen Bruzell, and Martin Andersson. "Bacterial biofilm elimination using gold nanorod localised surface plasmon resonance generated heat". In: *Materials Science and Engineering: C* 80 (2017), pp. 54–58. ISSN: 0928-4931. DOI: 10.1016/j.msec.2017.05.067.

[5] Alaaldin M. Alkilany et al. "Gold nanorods: Their potential for photothermal therapeutics and drug delivery, tempered by the complexity of their biological interactions". In: *Advanced Drug Delivery Reviews* 64.2 (2012). Biological Interactions of Nanoparticles, pp. 190–199. ISSN: 0169-409X. DOI: 10.1016/j.addr.2011.03.005.

[6] Ignacio de Miguel et al. "Plasmon-Based Biofilm Inhibition on Surgical Implants". In: *Nano Letters* 19.4 (2019), pp. 2524–2529. DOI: 10.1021/acs.nanolett.9b00187.

[7] Annette Erichsen Andersson et al. "Comparison between mixed and laminar airflow systems in operating rooms and the influence of human factors: Experiences from a Swedish orthopedic center". In: *American Journal of Infection Control* 42.6 (2014), pp. 665–669. ISSN: 0196-6553. DOI: 10.1016/j.ajic.2014.02.001.

[8] Rabih O. Darouiche et al. "Association of Airborne Microorganisms in the Operating Room With Implant Infections: A Randomized Controlled Trial". In: *Infection Control & Hospital Epidemiology* 38.1 (2017), pp. 3–10. DOI: 10.1017/ice.2016.240.

[9] Tim Sandle. "13 - Cleanrooms, isolators and cleanroom technology". In: *Sterility, Sterilisation and Sterility Assurance for Pharmaceuticals*. Ed. by Tim Sandle. Woodhead Publishing Series in Biomedicine. Woodhead Publishing, 2013,

pp. 189–207. ISBN: 978-1-907568-38-1. DOI: 10.1533/9781908818638.189.

[10] D. Chauveaux. "Preventing surgical-site infections: Measures other than antibiotics". In: *Orthopaedics & Traumatology: Surgery & Research* 101.1, Supplement (2015). 2014 Instructional Course Lectures (SoFCOT), S77–S83. ISSN: 1877-0568. DOI: 10.1016/j.otsr.2014.07.028.

[11] Evan M. Hetrick and Mark H. Schoenfisch. "Reducing implant-related infections: active release strategies". In: *Chem. Soc. Rev.* 35 (9 2006), pp. 780–789. DOI: 10.1039/B515219B.

[12] Yi-Chung Chang et al. "Rapid single cell detection of Staphylococcus aureus by aptamer-conjugated gold nanoparticles". In: *Scientific Reports* 3 (2013), p. 1863. DOI: 10.1038/srep01863.

[13] Steven Y. C. Tong et al. "Staphylococcus aureus Infections: Epidemiology, Pathophysiology, Clinical Manifestations, and Management". In: *Clinical Microbiology Reviews* 28.3 (2015), pp. 603–661. DOI: 10.1128/CMR.00134-14.

[14] Bradley D. Jett et al. "Simplified Agar Plate Method for Quantifying Viable Bacteria". In: *BioTechniques* 23.4 (1997), pp. 648–650. DOI: 10.2144/97234bm22.

[15] Uzma Azeem Awan et al. "Stable and reproducible synthesis of gold nanorods for biomedical applications: a comprehensive study". In: *IET Nanobiotechnology* 12.2 (2018), pp. 182–190. DOI: 10.1049/iet-nbt.2016.0220.

[16] Leonardo Scarabelli et al. "A "Tips and Tricks" Practical Guide to the Synthesis of Gold Nanorods". In: *The Journal of Physical Chemistry Letters* 6.21 (2015). PMID: 26538043, pp. 4270–4279. DOI: 10.1021/acs.jpclett.5b02123.

[17] Qingfeng Zhang et al. "Facet Control of Gold Nanorods". In: *ACS Nano* 10.2 (2016). PMID: 26795706, pp. 2960–2974. DOI: 10.1021/acsnano.6b00258.

[18] Jorge Pérez-Juste et al. "Gold nanorods: Synthesis, characterization and applications". In: *Coordination Chemistry Reviews* 249.17 (2005). 36th International Conference on Coordination Chemistry, Merida, Mexico, July 2004, pp. 1870–1901. ISSN: 0010-8545. DOI: 10.1016/j.ccr.2005.01.030.

[19] Xiaohua Huang, Svetlana Neretina, and Mostafa A. El-Sayed. "Gold Nanorods: From Synthesis and Properties to Biological and Biomedical Applications". In: *Advanced Materials* 21.48 (2009), pp. 4880–4910. DOI: 10.1002/adma.200802789.

[20] Enrique Carbó-Argibay et al. "The Crystalline Structure of Gold Nanorods Revisited: Evidence for Higher-Index Lateral Facets". In: *Angewandte Chemie International Edition* 49.49 (2010), pp. 9397–9400. DOI: 10.1002/anie.201004910.

[21] Hadas Katz-Boon et al. "Stability of Crystal Facets in Gold Nanorods". In: *Nano Letters* 15.3 (2015). PMID: 25658226, pp. 1635–1641. DOI: 10.1021/acs.nanolett.5b00124.

[22] Neyvis Almora-Barrios et al. “Theoretical Description of the Role of Halides, Silver, and Surfactants on the Structure of Gold Nanorods”. In: *Nano Letters* 14.2 (2014). PMID: 24397442, pp. 871–875. DOI: 10.1021/nl404661u.

[23] H. K. Jang et al. “Effects of chemical etching with nitric acid on glass surfaces”. In: *Journal of Vacuum Science & Technology A* 19.1 (2001), pp. 267–274. DOI: 10.1116/1.1333087.

[24] Vincenzo Amendola et al. “Surface plasmon resonance in gold nanoparticles: a review”. In: *Journal of Physics: Condensed Matter* 29.20 (Apr. 2017), p. 203002. DOI: 10.1088/1361-648x/aa60f3.

[25] Wonjin Jo and Min Jun Kim. “Influence of the photothermal effect of a gold nanorod cluster on biofilm disinfection”. In: *Nanotechnology* 24.19 (Apr. 2013), p. 195104. DOI: 10.1088/0957-4484/24/19/195104.

[26] Alaaldin M. Alkilany and Catherine J. Murphy. “Toxicity and cellular uptake of gold nanoparticles: what we have learned so far?” In: *Journal of Nanoparticle Research* 12 (7 2010), pp. 2313–2333. DOI: 10.1007/s11051-010-9911-8.

[27] Paresh Chandra Ray, Hongtao Yu, and Peter P. Fu. “Toxicity and Environmental Risks of Nanomaterials: Challenges and Future Needs”. In: *Journal of Environmental Science and Health, Part C* 27.1 (2009), pp. 1–35. DOI: 10.1080/10590500802708267.

[28] Alkilany A.M. and Murphy C.J. “Toxicity and cellular uptake of gold nanoparticles: what we have learned so far?” In: *Journal of Nanoparticle Research* 12 (2010), pp. 2313–2333. DOI: 10.1007/s11051-010-9911-8.

[29] Ellen E. Connor et al. “Gold Nanoparticles Are Taken Up by Human Cells but Do Not Cause Acute Cytotoxicity”. In: *Small* 1.3 (2005), pp. 325–327. DOI: 10.1002/smll.200400093.

[30] Shengnan Liao et al. “Improvement of Gold Nanorods in Photothermal Therapy: Recent Progress and Perspective”. In: *Frontiers in pharmacology* 12 (2021), pp. 1663–9812. DOI: 10.3389/fphar.2021.664123.

[31] Kannan M. Krishnan. *Principles of Materials Characterization and Metrology.* Oxford University Press, 2021. ISBN: 978-0-19-883025-2.

[32] Fred Rost. “Fluorescence Microscopy, Applications”. In: *Encyclopedia of Spectroscopy and Spectrometry.* Ed. by John C. Lindon, George E. Tranter, and David W. Koppenaal. Third Edition. Oxford: Academic Press, 2017, pp. 627–631. ISBN: 978-0-12-803224-4. DOI: 10.1016/B978-0-12-803224-4.00147-3.

[33] José-Angel Conchello Jeff Lichtman. “Fluorescence microscopy”. In: *Nat Methods* 2 (2005), pp. 910–919. DOI: 10.1038/nmeth817.

[34] W.William Wilson et al. “Status of methods for assessing bacterial cell surface charge properties based on zeta potential measurements”. In: *Journal of Microbiological Methods* 43.3 (2001), pp. 153–164. ISSN: 0167-7012. DOI: 10.1016/S0167-7012(00)00224-4.

[35] Douglas C. Montgomery. *Design and Analysis of Experiments (8th Edition).* John Wiley & Sons, 2013. ISBN: 978-1-118-14692-7.

A

Appendix

Appendix A includes calculations of the gold nanorod concentration used in the project, from UV-Vis-NIR spectroscopy and from theory. It also presents characteristics of the gold nanorod-functionalised glass that have a localized surface plasmon resonance frequency at 742 nm measured in air.

AI Calculation of the Gold Nanorod Concentration From UV-Vis-NIR Spectroscopy

An absorbance value of 1.2 at 400 nm corresponds to a concentration of 0.5 mM of Au(0). This allows the concentration of Au(0) to be calculated as

$$[Au(0)] = \frac{A_{400}}{1.2} * 0.5 * 10^{-3}$$

where A_{400} is the absorbance at 400 nm [16]. Assuming the gold nanorods are shaped as cylinders, the volume of a nanorod can be estimated by

$$V_{nanorods} = \pi * l * (\frac{w}{2})^2$$

where l and w are mean values of length and width of the gold nanorods, determined from image analysis of SEM micrographs. The mean values of the gold nanorods length and width are 68.32 nm and 18.21 nm.

Knowing both the concentration of Au(0) and the volume of a nanorod, the concentration of gold nanorods can be calculated by

$$[nanorods] = \frac{[Au(0)]*M_{Au(0)}}{\rho_{Au(0)}*V_{nanorods}*N_A}$$

where $M_{Au(0)}$ is the molar mass of gold (196.96 g/mole), $\rho_{Au(0)}$ is the density of gold ($19.32 \cdot 10^6$ g/m^3), and N_A is Avogadro's constant ($6.022 \cdot 10^{23}$ mole^{-1}). For an absorbance at 400 nm of 0.5, the concentration of the gold nanorods is

$$[nanorods] = \frac{\frac{0.5}{1.2}*0.5*10^{-3}*196.96}{19.32*10^6*\pi*68.32*10^{-9}*(\frac{18.21*10^{-9}}{2})^2*6.022*10^{23}} = 0.198 * 10^{-9} \text{ M}$$

AII Theoretical Calculation of the Gold Nanorod Concentration

The amount of Au(III) added to the seed solution from 25 µL of 50 mM gold(III) chloride trihydrate is

$$n^{seed}_{Au(III)} = 25 * 10^{-6}\ \text{L} * 0.05\ \text{M} = 1.25 * 10^{-6}\ \text{mole}$$

The total volume of the seed solution (V^{seed}_{tot}) is 5.025 mL containing 25 µL of gold(III) chloride trihydrate, 4.7 mL CTAB and 300 µL sodium borohydride solution. With the total seed solution volume and by assuming that 95 % of all Au(III) is reduced to Au(0), the concentration of Au(0) can be calculated.

$$[Au(0)]_{seed} = 0.95 * \frac{n^{seed}_{Au(III)}}{V^{seed}_{tot}} = 2.36 * 10^{-4}\ \text{M}$$

Further in the synthesis is 144 µL of the seed solution added to the growth solution. This volume corresponds to when the synthesis is scaled up 6 times the original volumes. The amount of Au(0) from the seed solution that is added to the growth solution is

$$n^{seed}_{Au(0)} = 144 * 10^{-6}\ \text{L} * 2.36 * 10^{-4}\ \text{M} = 34.03 * 10^{-9}\ \text{mole}$$

600 µL of 50 mM gold(III) chloride trihydrate is added to the growth solution. This volume is scaled up 6 times the original volume. With this volume and by assuming that 95 % of all Au(III) is reduced to Au(0), the amount of Au(0) in the growth solution can be calculated to be

$$n^{growth}_{Au(0)} = 0.95 * 600 * 10^{-6}\ \text{L} * 0.05\ \text{M} = 28.5 * 10^{-6}\ \text{mole}$$

The total amount of Au(0) in the synthesis is then

$$n^{tot}_{Au(0)} = n^{seed}_{Au(0)} + n^{growth}_{Au(0)} = 28.53403 * 10^{-6}\ \text{mole}$$

Assuming the gold nanorods are shaped as cylinders, the volume of a nanorod can be estimated by

$$V_{nanorods} = \pi * l * \frac{w}{2}^2$$

where l and w are mean values of length and width of the gold nanorods, determined from image analysis of SEM micrographs. The mean values of the gold nanorods length and width are 68.32 nm and 18.21 nm. With the total amount of Au(0) and the volume of the nanorods, the amount of the gold nanorods can be calculated by

$$n_{nanorods} = \frac{n^{tot}_{Au(0)} * M_{Au(0)}}{\rho_{Au(0)} * V_{nanorods} * N_A} = 27.15 * 10^{-12}\ \text{mole}$$

where $M_{Au(0)}$ is the molar mass of gold (196.96 g/mole), $\rho_{Au(0)}$ is the density of gold ($19.32 \cdot 10^6$ g/m^3), and N_A is Avogadro's constant ($6.022 \cdot 10^{23}$ mole^{-1}). The concentration of gold nanorods in the dispersion can then be calculated by

$$[nanorods]_{purified} = \frac{n_{nanorods}}{V}$$

where V is the volume of Milli-Q water used to redisperse the gold nanorods after the last purification step.

A volume of 5 mL is used to redisperse the gold nanorods after the last purification step. With this volume and by assuming that 30 % of the gold nanorods are washed away during the purification, the concentration of the nanorods can be calculated.

$$[nanorods]_{purified} = \frac{27.15*10^{-12}}{0.005} * 0.7 = 3.8 * 10^{-9} \text{ M}$$

2 mL of this dispersion is then used in UV-Vis-NIR spectroscopy, where a total volume of 36 mL Milli-Q water is added for the dispersion to show an absorbance of 0.5 at 400 nm. The final concentration of the gold nanorod dispersion can then be calculated.

$$[nanorods] = \frac{3.8*10^{-9}*0.002}{0.038} = 0.20 * 10^{-9} \text{ M}$$

AIII Gold Nanorod-Functionalised Glass With a Localised Surface Plasmon Resonance Frequency at 742 nm in Air

The gold nanorod-functionalised glass surface produced during previous work in the research group are called AuNR-Glass^{742}. These surfaces show a LSPR frequency of approximately 742 nm measured in air. The average surface coverage of AuNR-Glass^{742} is 15.3 ± 0.9 % corresponding to 104 nanorods/µm^2. A representative SEM micrograph is presented in Figure A1. The average length, width and aspect ratio of the gold nanorods on these surfaces is 69.4 nm, 21.3 nm and 3.33 respectively.

Localised surface plasmon resonance (LSPR) spectra of AuNR-Glass^{742} and of gold nanorods dispersed in Milli-Q water (AuNR^{742}) are presented in Figure A2. The spectral data is normalised for both AuNR-Glass^{742} and AuNR^{742}. The surfaces measured in air showed a longitudinal absorption band at approximately 722-762 nm, with a peak at 742 nm. The gold nanorods used to produce the surfaces shows, dispersed in Milli-Q water, a long longitudinal absorption band at approximately 798-839 nm, with a peak at 818 nm. The shift that occurs when the gold nanorods are measured in air immobilised on glass compared to free in water is approximately 76 nm.

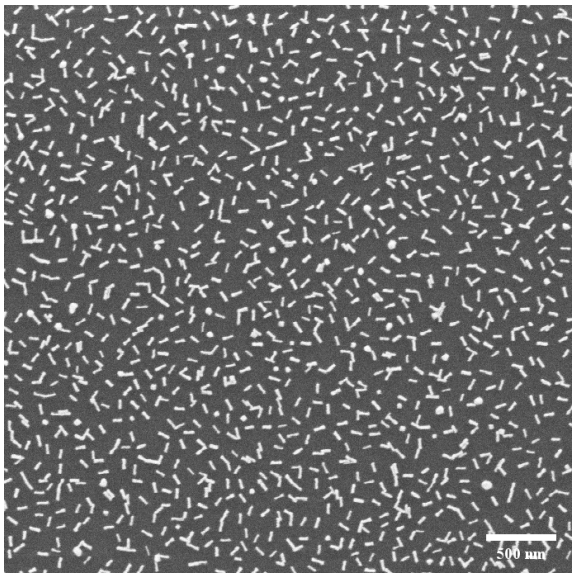

Figure A1: Scanning electron microscopy micrograph at 50 000x magnification of gold nanorod- functionalised glass with a localised surface plasmon resonance frequency of 742 nm measured in air

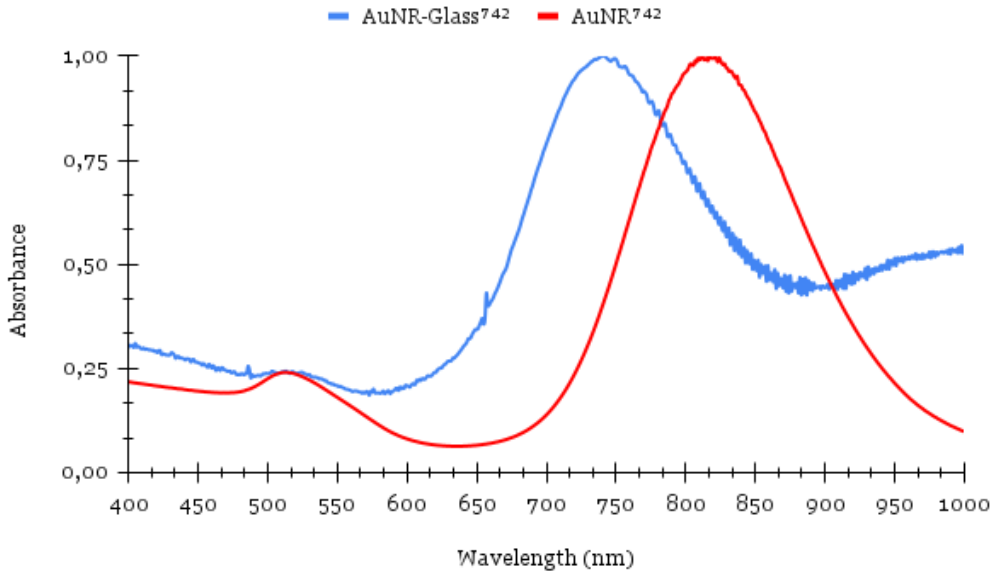

Figure A2: Localised surface plasmon resonance spectra of gold nanorod-functionalised glass measured in air (AuNR-Glass^{742}) and gold nanorods measured in Milli-Q water (AuNR^{742})

B

Appendix

Appendix B includes p-values of the t-tests from both *in vitro* studies. It also presents results of CFU, example of statistical calculations of the 2^2 factorial design and ANOVA tables from the microbial contamination trials.

BI Colony-Forming Unit From the Microbial Contamination Trials

Example pictures of agar plates with colonies from the microbial contamination trials are presented in Figure B1.

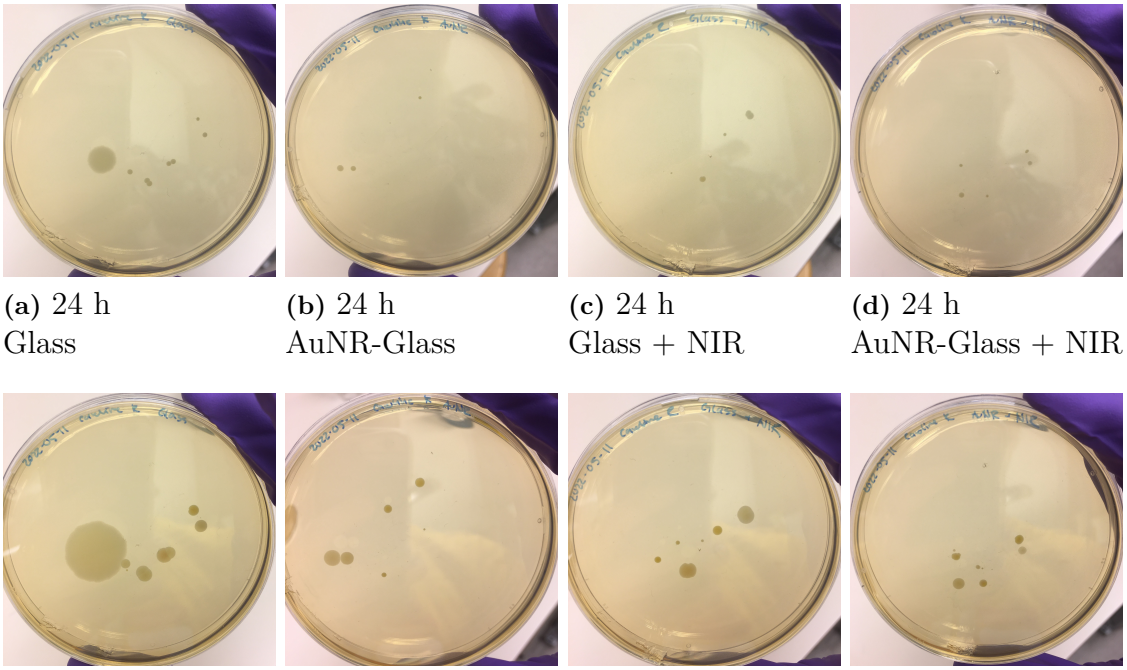

(a) 24 h Glass | **(b)** 24 h AuNR-Glass | **(c)** 24 h Glass + NIR | **(d)** 24 h AuNR-Glass + NIR

(e) 48 h Glass | **(f)** 48 h AuNR-Glass | **(g)** 48 h Glass + NIR | **(h)** 48 h AuNR-Glass + NIR

Figure B1: Example pictures of agar plates with colonies after 24 h and 48 h from the trial with near-infrared light at 15 W

Colony-forming unit (CFU) for the microbial contamination trials are presented in Table B1 and B2 below. Table B1 show the fist trial using NIR light at 10 W and Table B2 show the second trial using NIR light at 15 W. CFU is presented for both 24 h and 48 h. CFU counted after 45 h is shown in parenthesis. The groups used for the trials were bare glass surfaces (Glass), gold nanorod-functionalised glass surfaces (AuNR-Glass), NIR light irradiated bare glass surfaces (Glass + NIR) and NIR light irradiated gold nanorod-functionalised glass surfaces (AuNR-Glass + NIR). The NIR light used had a spectral output of 808 ± 3 nm. Three replicates of each surface group were used in the trial with NIR light at 10 W. For the trial with NIR light at 15 W were six replicates of each surface group used.

Table B1: Colony-forming unit (CFU) after 24 h and 48 h, where CFU after 48 h is shown in parenthesis, for bare glass surfaces (Glass) and gold nanorod-functionalised glass surfaces (AuNR-Glass), either non-irradiated or irradiated with 10 W at 808 nm (+ NIR)

Surface	**Replicate**		
	I	**II**	**III**
Glass	5 (9)	3 (4)	6 (8)
AuNR-Glass	5 (17)	2 (6)	8 (15)
Glass + NIR	6 (6)	3 (5)	4 (8)
AuNR-Glass + NIR	9 (9)	4 (7)	10 (13)

Table B2: Colony-forming unit (CFU) after 24 h and 48 h, where CFU after 48 h is shown in parenthesis, for bare glass surfaces (Glass) and gold nanorod-functionalised glass surfaces (AuNR-Glass), either non-irradiated or irradiated with 15 W at 808 nm (+ NIR)

Surface	**Replicate**					
	I	**II**	**III**	**IV**	**V**	**VI**
Glass	8 (9)	7 (10)	10 (10)	6 (8)	13 (14)	3 (4)
AuNR-Glass	26 (30)	5 (6)	20 (22)	8 (12)	12 (18)	7 (9)
Glass + NIR	18 (21)	13 (15)	4 (6)	22 (26)	5 (9)	10 (15)
AuNR-Glass + NIR	5 (7)	7 (11)	10 (12)	13 (15)	7 (9)	11 (15)

BII P-Values of the T-Tests for the Microbial Contamination Trials

P-values of the t-tests are presented for the microbial contamination trials in this section. The different surface groups used for the microbial contamination trials

were bare glass surfaces (Glass), gold nanorod-functionalised glass surfaces (AuNR-Glass), near-infrared (NIR) light irradiated bare glass surfaces (Glass + NIR) and NIR light irradiated gold nanorod-functionalised glass surfaces (AuNR-Glass + NIR). The t-tests were made to evaluate if there were any significant difference among population means between the groups. The groups compared in the t-tests were Glass and AuNR-Glass, Glass and Glass + NIR, and AuNR-Glass and AuNR-Glass + NIR. P-values from the microbial contamination trial with NIR light of 10 W are presented in Table B3, and P-values from the trial with NIR light of 15 W are presented in Table B4.

Table B3: P-values of each t-test for the microbial contamination trial using near-infrared light at 10 W

Groups	**P-Value**	
	24 h	**48 h**
Glass AuNR-Glass	0.8722	0.2016
Glass Glass + NIR	0.8025	0.7247
AuNR-Glass AuNR-Glass + NIR	0.3528	0.4756

Table B4: P-values of each t-test for the microbial contamination trial using near-infrared light at 15 W

Groups	**P-value**	
	24 h	**48 h**
Glass AuNR-Glass	0.1889	0.1020
Glass Glass + NIR	0.2260	0.0910
AuNR-Glass AuNR-Glass + NIR	0.2740	0.2571

BIII Statistical Calculations for the Microbial Contamination Trials

In this section is an example of statistical calculations using a 2^2 factorial design for the microbial contamination trials presented. In the example data from the trial

with near-infrared (NIR) light irradiation at 10 W and colony-forming unit (CFU) counted after 48 h is used.

A 2^2 factorial design has two factors, A and B, each run at two levels. The levels of the factor are either "high" or "low" [35]. For this project, the type of surface is factor A, with the high level denoting a gold nanorod-functionalised glass surface (AuNR-Glass) and the low level denoting a bare glass surface (Glass). The treatment is factor B and the two levels are either irradiation with NIR light (+ NIR) or no irradiation. In the microbial contamination trial with NIR light irradiation at 10 W the experiment was replicated three times giving a total of 12 runs. The data obtained for the microbial contamination trial with NIR light irradiation at 10 W and CFU counted after 48 h is presented in Table B5.

Table B5: The data obtained for the microbial contamination trial with near-infrared light irradiation at 10 W and colony-forming unit counted after 48 h

Factor			**Combination**	**Replicate**			**Total**
A	**B**	**AB**		**I**	**II**	**III**	
-	-	+	Glass	9	4	8	21
+	-	-	AuNR-Glass	17	6	15	38
-	+	-	Glass + NIR	6	5	8	19
+	+	+	AuNR-Glass + NIR	9	7	13	29

The four combinations in the design are represented by lowercase letters. a represents the combination of A at the high level and B at the low level (AuNR-Glass), b represents A at the low level and B at the high level (Glass + NIR), and ab represents both factors at the high level (AuNR-Glass + NIR). Often (1) is used to represent both factors at the low level (Glass). (1), a, b, and ab represent the total response, in this case CFU values, at all n replicates taken at the combination. The average effect of a factor is the change in response produced by a change in the level of that factor averaged over the level of the other factors. The effect of A at the low level of B is [a - (1)]/n and the effect of A at the high level of B is [ab - b]/n [35]. Taking the average of these gives the main effect of A as

$$A = \frac{1}{2n}[ab + a - b - (1)] = \frac{1}{2*3}[29 + 38 - 19 - 21] = 4.5$$

In the same way is the average effect of B found as

$$B = \frac{1}{2n}[ab + b - a - (1)] = \frac{1}{2*3}[29 + 19 - 38 - 21] = -1.83$$

The interaction effect of AB is can be defined as the average difference between the effect of A at the high level of B and the effect of A at the low level of B. Thus,

$$AB = \frac{1}{2n}[ab + (1) - a - b] = \frac{1}{2*3}[29 + 21 - 38 - 19] = -1.17$$

The factor effects for the two different trials and for both CFU counting times are presented below in Table B6.

Table B6: The factor effects for both microbial contamination trials (near-infrared light irradiation at 10 W or 15 W) with colony-forming unit counted after 24 h and 48 h

Average	**10 W**		**15 W**	
Effects	**24 h**	**48 h**	**24 h**	**48 h**
A	1.83	4.50	1	1.58
B	1.17	-1.83	0	0.75
AB	1.50	-1.17	-4.17	-5.42

For the trial with 10 W and CFU counted after 48 h is the effect of A (surface type) positive. This suggests that going from the low level of A (Glass) to the high level (AuNR-Glass) will increase the yield of CFU. The effect of B (treatment) is negative and is suggesting that going from the low level of B (no NIR) to the high level (+ NIR) will decrease the yield of CFU. The interaction effect AB is negative. This suggest that going from the low level of AB (AuNR-Glass and Glass + NIR) to the high level (Glass and AuNR-Glass + NIR) will decrease the yield of CFU. The interpretations of the factor effects can be confirmed or rejected by using analysis of variance. The sum of square for A, B, and AB is calculated by

$$SS_A = \frac{[ab+a-b-(1)]^2}{4n} = \frac{[29+38-19-21]^2}{4*3} = 60.75$$

$$SS_B = \frac{[ab+b-a-(1)]^2}{4n} = \frac{[29+19-38-21]^2}{4*3} = 10.08$$

$$SS_{AB} = \frac{[ab+(1)-a-b]^2}{4n} = \frac{[29+21-38-19]^2}{4*3} = 4.08$$

and the total sum of squares with $4n-1$ degrees of freedom is

$$SS_T = \sum_{i=1}^{2}\sum_{j=1}^{2}\sum_{k=1}^{n} y_{ijk}^2 - \frac{y_{...}^2}{4n} = 180.91$$

The error sum of squares, with $4(n-1)$ degrees of freedom can then be calculated.

$$SS_E = SS_T - SS_A - SS_B - SS_{AB} = 106$$

The complete analysis of variance (ANOVA) table is presented in Appendix BIV in Table B8. The P-value for A (surface type), B (treatment) and AB (interaction) is 0.0647, 0.4084 and 0.5940 respectively. A is significant at a 90 % significance level and the effect of A indicates that that going from the low level (Glass) to the high level (AuNR-Glass) will increase the yield of CFU, independent of the levels of factor B. Thus, a surface with gold nanorods is more likely to exhibit a higher CFU compared to a bare glass surface. The other interpretations of the factor effects can be rejected since they are not shown significant.

BIV Analysis of Variance Tables for the Microbial Contamination Trials

Analysis of variance (ANOVA) tables are presented for the two different trials for colony-forming unit counted after 24 h and 48 h. For the trial with near-infrared light at 10 W see Table B7 and B8. The ANOVA tables for the trial with 15 W are presented in Table B9 and B10.

Table B7: ANOVA table for the microbial contamination trial with near-infrared light irradiation at 10 W with colony-forming unit counted after 24 hours

Source of Variation	**Sum of Squares**	**Degrees of Freedom**	**Mean Square**	$\mathbf{F}_q$	**P-value**
Surface	10.08	1	10.08	1.68	0.2310
Treatment	4.08	1	4.8	0.68	0.4333
Interaction	6.75	1	6.75	1.13	0.3198
Error	48.00	8	6.00		
Total	68.92	11			

Table B8: ANOVA table for the microbial contamination trial with near-infrared light irradiation at 10 W with colony-forming unit counted after 48 hours

Source of Variation	**Sum of Squares**	**Degrees of Freedom**	**Mean Square**	$\mathbf{F}_q$	**P-value**
Surface	60.75	1	60.75	4.58	0.0647
Treatment	10.08	1	10.08	0.76	0.4084
Interaction	4.08	1	4.08	0.31	0.5940
Error	106.00	8	13.25		
Total	180.92	11			

Table B9: ANOVA table for the microbial contamination trial with near-infrared light irradiation at 15 W with colony-forming unit counted after 24 hours

Source of Variation	**Sum of Squares**	**Degrees of Freedom**	**Mean Square**	$\mathbf{F}_q$	**P-value**
Surface	6.00	1	6.00	0.17	0.6836
Treatment	0.00	1	0.00	0.00	1.0000
Intreaction	104.17	1	104.17	2.97	0.1003
Error	701.67	20	35.08		
Total	811.83	23			

Table B10: ANOVA table for the microbial contamination trial with near-infrared light irradiation at 15 W with colony-forming unit counted after 48 hours

Source of Variation	Sum of Squares	Degrees of Freedom	Mean Square	F_q	P-value
Surface	15.04	1	15.04	0.39	0.5412
Treatment	3.38	1	3.38	0.09	0.7714
Intreaction	176.04	1	176.04	4.52	0.0461
Error	778.50	20	38.93		
Total	972.96	23			

BV P-Values of the T-Tests for the *In Vitro* Study With Bacteria Cultured on Gold Nanorod-Functionalised Glass

P-values of the t-tests for the *in vitro* study with *Staphylococcus aureus* cultured on gold nanorod-functionalised glass are presented in Table B11. Gold nanorod-functionalised glass with a LSPR frequency in air at 795 nm (AuNR-Glass) and gold nanorod-functionalised glass with a LSPR frequency in air at 742 nm (AuNR-Glass^{742}) were used in this study. Three different surface groups were analysed in the study. AuNR-Glass, AuNR-Glass irradiated with NIR light at 15 W for 5 seconds (AuNR-Glass + NIR) and AuNR-Glass^{742} irradiated with NIR light at 15 W for 5 seconds (AuNR-Glass^{742} + NIR).

Table B11: P-values of each t-test for the *in vitro* study with bacteria cultured on gold nanorod-functionalised glass

Groups	P-value
AuNR-Glass AuNR-Glass + NIR	0.0382
AuNR-Glass AuNR-Glass742 + NIR	0.0122
AuNR-Glass + NIR AuNR-Glass^{742} + NIR	0.9985

DEPARTMENT OF CHEMISTRY AND CHEMICAL ENGINEERING
CHALMERS UNIVERSITY OF TECHNOLOGY
Gothenburg, Sweden
www.chalmers.se

CHALMERS
UNIVERSITY OF TECHNOLOGY